U.S. Department
of Transportation

Federal Railroad
Administration

The Development and Application of Rail Defect Fracture Models to Assess Remedial Actions

Office of Research
and Development
Washington, DC 20590

Ronald A. Mayville
Richard G. Stringfellow

Arthur D. Little, Inc.
Acorn Park
Cambridge, MA 02140-2390

REPORT DOCUMENTATION PAGE		Form Approved OMB No. 0704-0188

Public reporting burden for this collection of information is estimated to average 1 hour per response, including the time for reviewing instructions, searching existing data sources, gathering and maintaining the data needed, and completing and reviewing the collection of information. Send comments regarding this burden estimate or any other aspect of this collection of information, including suggestions for reducing this burden, to Washington Headquarters Services, Directorate for Information Operations and Reports, 1215 Jefferson Davis Highway, Suite 1204, Arlington, VA 22202-4302, and to the Office of Management and Budget, Paperwork Reduction Project (0704-0188), Washington, DC 20503.

1. AGENCY USE ONLY (Leave blank)	2. REPORT DATE August 1993	3. REPORT TYPE AND DATES COVERED Final Report - June 1991-January 1993

4. TITLE AND SUBTITLE The Development and Application of Rail Defect Fracture Models to Assess Remedial Actions	5. FUNDING NUMBERS RR328/R3026
6. AUTHOR(S) Ronald A. Mayville and Richard G. Stringfellow	DTRS-57-89-D-00007 VA1032

7. PERFORMING ORGANIZATION NAME(S) AND ADDRESS(ES) Arthur D. Little, Inc.* Acorn Park Cambridge, MA 02140-2390	8. PERFORMING ORGANIZATION REPORT NUMBER DOT-VNTSC-FRA-93-12

9. SPONSORING/MONITORING AGENCY NAME(S) AND ADDRESS(ES) U.S. Department of Transportation Federal Railroad Administration Office of Research and Development 400 7th Street, SW Washington, DC 20590	10. SPONSORING/MONITORING AGENCY REPORT NUMBER DOT/FRA/ORD-93/33

11. SUPPLEMENTARY NOTES *under contract to:	U.S. Department of Transportation Research and Special Programs Administration Volpe National Transportation Systems Center Cambridge, MA 02142

12a. DISTRIBUTION/AVAILABILITY STATEMENT This document is available to the public through the National Technical Information Service, Springfield, VA 22161	12b. DISTRIBUTION CODE

13. ABSTRACT (Maximum 200 words)

The fracture mechanics models were refined for two types of rail defects - the bolt hole crack and the vertical split head. Beam-type finite element analysis was conducted to determine the effects of joint bar looseness, rail height mismatch and train speed on the static and dynamic components of the crack driving force for the bolt hole crack. Both two- and three-dimensional finite element analyses were conducted to determine the Modes I and II stress intensities for a kinked vertical split head crack. The results from these analyses were reviewed to determine their implication on remedial actions.

14. SUBJECT TERMS rail defect, crack, bolt hole, vertical split head, dynamic load			15. NUMBER OF PAGES 74
			16. PRICE CODE

17. SECURITY CLASSIFICATION OF REPORT Unclassified	18. SECURITY CLASSIFICATION OF THIS PAGE Unclassified	19. SECURITY CLASSIFICATION OF ABSTRACT Unclassified	20. LIMITATION OF ABSTRACT

PREFACE

Remedial actions are specified by the Federal Railroad Administration (FRA) for cases in which defects or cracks are discovered in rails. The actions taken, which include slow orders, temporary repairs and defect size monitoring, depend on the track class and size of the defect. For example, detail fractures over 20% of the head area require the application of joint bars. The remedial actions are apparently based on experience.

Models from the field of fracture mechanics have become available over the last few years that can be used to assess the effectiveness and implications of the remedial actions. These models cover the detail fracture, bolt hole crack and vertical split head. In a previous report [1], application of these models to the assessment of remedial actions revealed some important shortcomings of the bolt hole crack and vertical split head fracture mechanics models.

This report addresses these shortcomings by continuing the development of the models. Several finite element calculations are carried out to investigate the effect that loose joint bars have on dynamic loads and crack driving forces for the bolt hole crack and of a realistic vertical split head crack geometry on fatigue crack growth and fracture behavior of this defect.

METRIC/ENGLISH CONVERSION FACTORS

ENGLISH TO METRIC

LENGTH (APPROXIMATE)

1 inch (in) = 2.5 centimeters (cm)

1 foot (ft) = 30 centimeters (cm)

1 yard (yd) = 0.9 meter (m)

1 mile (mi) = 1.6 kilometers (km)

AREA (APPROXIMATE)

1 square inch (sq in, in^2) = 6.5 square centimeters (cm^2)

1 square foot (sq ft, ft^2) = 0.09 square meter (m$_2$)

1 square yard (sq yd, yd^2) = 0.8 square meter (m^2)

1 square mile (sq mi, mi^2) = 2.6 square kilometers (km^2)

1 acre = 0.4 hectares (he) = 4,000 square meters (m^2)

MASS - WEIGHT (APPROXIMATE)

1 ounce (oz) = 28 grams (gr)

1 pound (lb) = .45 kilogram (kg)

1 short ton = 2,000 pounds (lb) = 0.9 tonne (t)

VOLUME (APPROXIMATE)

1 teaspoon (tsp) = 5 milliliters (ml)

1 tablespoon (tbsp) = 15 milliliters (ml)

1 fluid ounce (fl oz) = 30 milliliters (ml)

1 cup (c) = 0.24 liter (1)

1 pint (pt) = 0.47 liter (1)

1 quart (qt) = 0.96 liter (1)

1 gallon (gal) = 3.8 liters (1)

1 cubic foot (cu ft, ft^3) = 0.03 cubic meter (m^3)

1 cubic yard (cu yd, yd^3) = 0.76 cubic meter (m^3)

TEMPERATURE (EXACT)

[(x-32)(5/9)] ^{o}F = y ^{o}C

METRIC TO ENGLISH

LENGTH (APPROXIMATE)

1 millimeter (mm) = 0.04 inch (in)

1 centimeter (cm) = 0.4 inch (in)

1 meter (m) = 3.3 feet (ft)

1 meter (m) = 1.1 yards (yd)

1 kilometer (km) = 0.6 mile (mi)

AREA (APPROXIMATE)

1 square centimeter (cm^2) = 0.16 square inch (sq in, in^2)

1 square meter (m^2) = 1.2 square yeards (sq yd, yd^2)

1 square kilometer (km^2) = 0.4 square mile (sq mi, mi^2)

1 hectare (he) = 10,000 square meters (m^2) = 2.5 acres

MASS - WEIGHT (APPROXIMATE)

1 gram (gr) = 0.036 ounce (oz)

1 kilogram (kg) = 2.2 pounds (lb)

1 tonne (t) = 1,000 kilograms (kg) = 1.1 short tons

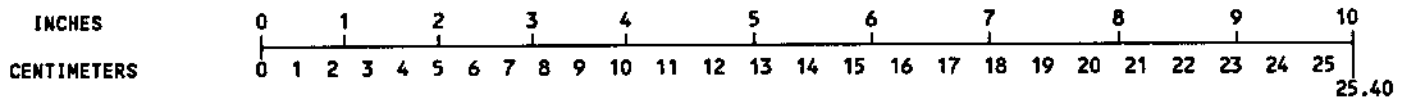#### VOLUME (APPROXIMATE)

1 milliliters (ml) = 0.03 fluid ounce (fl oz)

1 liter (1) = 2.1 pints (pt)

1 liter (1) = 1.06 quarts (qt)

1 liter (1) = 0.26 gallon (gal)

1 cubic meter (m^3) = 36 cubic feet (cu ft, ft^3)
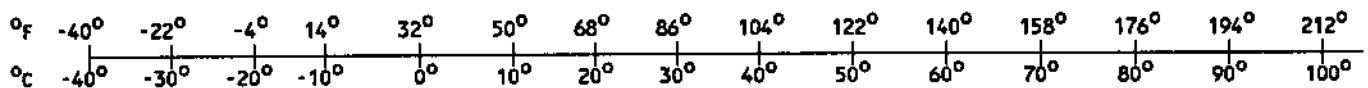
1 cubic meter (m^3) = 1.3 cubic yards (cu yd, yd^3)

TEMPERATURE (EXACT)

[(9/5) y + 32] ^{o}C = x ^{o}F

QUICK INCH-CENTIMETER LENGTH CONVERSION

INCHES   0   1   2   3   4   5   6   7   8   9   10

CENTIMETERS 0 1 2 3 4 5 6 7 8 9 10 11 12 13 14 15 16 17 18 19 20 21 22 23 24 25
                                                                            25.40

QUICK FAHRENHEIT-CELSIUS TEMPERATURE CONVERSION

^{o}F -40° -22° -4° 14° 32° 50° 68° 86° 104° 122° 140° 158° 176° 194° 212°

^{o}C -40° -30° -20° -10° 0° 10° 20° 30° 40° 50° 60° 70° 80° 90° 100°

For more exact and or other conversion factors, see NBS Miscellaneous Publication 286, Units of Weights and Measures. Price $2.50. SD Catalog No. C13 10286.

TABLE OF CONTENTS

LIST OF FIGURES

LIST OF TABLES

LIST OF ABBREVIATIONS AND SYMBOLS

b - beam width

f - natural frequency

h - beam height

I_{jb} - moment of inertia of both joint bars

I_r - moment of inertia of the rail

K_I - Mode I stress intensity factor

K_{II} - Mode II stress intensity factor

K_c - fracture toughness

ℓ - free length of the beam - joint efficiency factor

M - the moment in the joint bars at the center of the bolted joint

M_o - bending moment in continuous rail

m - unsprung wheelset mass

P_o - static wheel load

P_1 - peak wheel load corresponding to contact response after a bolted joint is crossed

P_2 - peak wheel load corresponding to track response after a bolted joint is crossed

R - wheel radius

t - time

u - foundation modulus

V - train speed

V_o - vertical wheel velocity

V_b - shear force in rail at location of first bolt hole

W - plastic collapse load

x - distance from joint

α_1 - bolted joint dip angle on the trailing edge

α_2 - bolted dip angle on the leading edge

Δ_g - joint bar/rail gap size

Δ_y - vertical displacement of rail

LIST OF ABBREVIATIONS AND SYMBOLS (continued)

δ - rail height mismatch

θ - top, vertical split head crack angle

σ_f - plastic flow stress

τ - duration of contact under impact conditions

ζ - non-dimensional damping coefficient

EXECUTIVE SUMMARY

A previous study to assess currently specified remedial actions with rail defect fracture mechanics models showed that models for the bolt hole crack and the vertical split head require further development. In particular, a better model was required to estimate the crack driving force for a bolt hole crack when the joint bars loosen. More accurate calculations were also needed for the form of the vertical split head most commonly observed in service, which includes an angled crack segment near the running surface.

Finite element analysis was used to further develop both models. A beam element model was used to simulate the interaction that occurs between the joint bars, rail ends and the foundation. The model accounted for looseness by simulating gaps of varying sizes between rail and joint bars. Static calculations for a tight joint showed that this model provides the same results as a model based on the mechanics developed by the Talbot committee. Static calculations also showed that the shear force at the bolt hole, which is the primary driving force for crack growth, decreases approximately 20% when the gap changes from zero to 0.010 inches. The joint efficiency factor, which is the ratio of the load carrying capacity of the joint to that of a continuous rail, was also calculated.

A set of dynamic calculations was carried out for both tight and loose joints and for varying degrees of rail end height mismatch. The modal analysis feature of the finite element program was used to determine the peak wheel load and peak, positive shear force at the first bolt hole for two rail sizes, 100 and 132 lb/yd, and two train speeds, 10 and 60 mph. Damping was also included. The results showed that the positive shear force at the bolt hole, which drives the most commonly observed bolt hole crack, is very sensitive to the contact conditions between the joint bar and rail. Generally, our calculations showed that this shear force increases as the gap between rail and joint bar increases to 0.010 inches, but then decreases with a further increase in gap size. On the other hand, the peak wheel load increases monotonically with gap size. The reason for the rise and then fall of positive bolt hole shear force can be traced to rail/joint bar and wheel/rail contact conditions at impact which change substantially with gap size. These results highlight the sensitivity of the model to the assumed contact geometry.

Two- and three-dimensional finite element analysis were used to calculate stress intensity factors for the vertical split head with top angled crack segment. The purpose of the two-dimensional analysis, which does not properly simulate the loading on this geometrically two-dimensional defect, was to select a load location and top crack segment angle for the three-dimensional analysis. Calculations showed that the greatest Mode I stress intensity at the top crack tip was obtained when the wheel load was applied at

the rail head corner opposite the side to which the angled segment points. The crack segment angle, which was varied from 20 to 40° to the horizontal, had essentially no effect on the stress intensity factor regardless of load location.

Based on these results, three-dimensional calculations were carried out with a 30° angled crack segment for a load applied at the corner of the rail head. These results show that the Mode I stress intensity at the tip of the angled crack is approximately 7 ksi$\sqrt{in}$. This value is in the threshold fatigue crack growth regime and explains why observed vertical growth from these defects is so slow. In fact, we estimate that over 200 MGT are required to cause breakout to the running surface of the most commonly observed defect size. This suggests that there is generally sufficient time to replace a rail that contains a vertical split head and that during this time there is little additional risk of fracture.

Analytical calculations were also carried out to estimate a lower bound on the critical crack length of the vertical split head. The results indicate that the critical length is over 4 inches when the defect is located at the end of a rail and over 14 inches when it is not. These lengths are greater than the current range of defect lengths specified in the remedial actions.

1. INTRODUCTION

Recently, a study was conducted to determine if predictions from fracture mechanics models developed over the last 10 years are consistent with remedial actions that are required when defects are discovered in railroad rails. Models for the detail fracture, the bolt hole crack and the vertical split head were used to assess the likelihood of fracture for such conditions as train speed, defect size, and time or amount of traffic. These are the primary variables from which specific remedial actions are determined. For example, if a vertical split head is discovered, the maximum speed must be reduced to 60 mph for a defect length of less than two inches. For a defect between two and four inches long the speed must be reduced to 30 mph. The study sought to establish whether these two conditions resulted in a comparable likelihood of fracture.

Generally, the remedial actions currently specified were found to be supported by the fracture mechanics models. Larger defects tend to grow faster with time and with greater train speed, which usually results in higher loads to the rail. Thus, reducing speed and interim inspection intervals have a clear and quantifiable benefit on reducing the risk of fracture.

However, in some cases, conclusions reached in the previous study were uncertain because of the state of development of the fracture mechanics models for two of the defects: the bolt hole crack and the vertical split head. Specifically, very simple models were used to treat the degree of joint bar looseness and the dynamic effects of a wheel crossing the joint. The model for the vertical split head was even less developed. Most of the research for this defect had been directed at the early stages of growth, for which the crack is entirely confined to a vertical plane. Most defects found in the field are characterized by an angled crack segment near the running surface (the top of the rail head.)

The objective of the study reported here was to continue development of the fracture mechanics models for the bolt hole crack and the vertical split head, specifically addressed at the weaknesses discussed above.

Finite element analysis was the primary tool used to further develop the models. A beam element model was developed for the bolt hole crack to simulate contact between joint bar and rail ends and to study such variables as the gap between rail and joint bar and wheel impact velocity. The effect of rail end height mismatch was also studied even though this is not specifically treated in the remedial action section of the track standards. Two- and three-dimensional finite element analysis was conducted for the vertical split head to determine the stress intensity factors for the angled crack.

The results show that dynamic wheel loads and the shear force at the bolt hole – which is the crack driving force – can be related to the unloaded gap between the joint bar and rail. A relationship has also been determined between this gap and the joint efficiency factor, which had been used arbitrarily in previous studies to characterize joint looseness. Results from rail height mismatch studies indicate that the bolt hole crack driving force increases only 10% when the mismatch height is increased from 0.25 to 0.50 inches and the train speed is 10 mph.

Vertical split head analyses show that fatigue from the top, angled crack will occur if the wheel is located at the corner of the rail head opposite the side toward which the angled crack points. However, the alternating stress intensity factor is in the threshold range and a large amount of traffic appears to be required to cause breakout to the running surface.

The next two sections of this report describe the model improvement and application efforts in detail. Section 4 provides a brief summary of the implications of the results on remedial actions.

2. BOLT HOLE CRACK

2.1 BACKGROUND

The current understanding of the fatigue crack growth and fracture behavior of bolt hole cracks is based largely on analytical studies and laboratory experiments. One of the primary conclusions of these investigations is that the shear force at the bolt hole of interest represents the crack driving force.

In prior work [1], an analytical model was developed to calculate the shear force acting at the bolt hole of interest. The forces acting at the end of a rail in a bolted joint consist of the loads applied by the joint bars, the track foundation and, if applicable, the wheel, Figure 2-1. Joint bar forces were obtained using the results of the Talbot committee [2], which discovered that the stresses in the joint bars could be generally explained by the application of two point loads on each side of the joint: one force directly adjacent to the joint acting, for a positive moment (rail base in tension), underneath the rail head, and another force near the end of the joint bar acting on the rail base. Once the locations of application of these forces were known, their magnitude was determined by equilibrium with a knowledge of the moment and shear force that act on the joint bars at the center of the joint. Moment and shear force were obtained by first calculating the values that would exist at the joint center if the rail were modeled as an infinite beam on an elastic foundation, and then multiplying these values by a joint efficiency factor, which is less than one. Given the joint bar forces and wheel load, the shear force at the bolt hole of interest was then determined by solving the equation for a semi-infinite beam-on-elastic foundation for this set of loads. In the prior analysis, the wheel load was multiplied by a dynamic amplification factor to account for the increase in load caused by the joint discontinuity.

The inclusion of the joint efficiency and dynamic amplification factors in this analysis seems to be quite important. Lack of fit or loosening of bolts due to relaxation and wear inevitably lead to gaps between the joint bars and rails. Associated with these gaps is a reduction in the ability of the joint to transfer bending moment [2] and, presumably, shear force. Thus, to model the joint as ideally tight and smooth appears unrealistic for the problem at hand. An understanding of the effect of train speed on dynamic wheel loads is also essential not only because this parameter is key to the remedial actions, but because of its variability in practice.
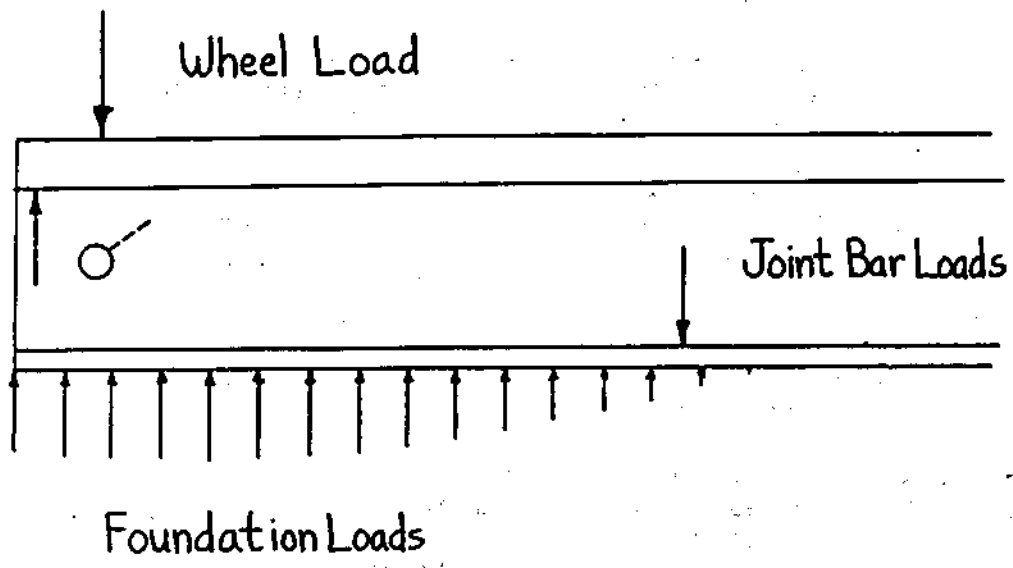
FIGURE 2-1. **ILLUSTRATION OF THE LOADS THAT ACT AT THE END OF A RAIL IN A BOLTED JOINT**

Prior to the present work, the joint efficiency factor was varied arbitrarily below a value felt to be the upper limit which, is given by [3]:

$$k = (I_{jb}/I_r)^{1/4},$$

where I_{jb} and I_r are the moments of inertia of both joint bars and the rail, respectively, about a horizontal axis in the plane of the rail cross section. For example, the value of k for a 132 lb/yd rail system is 0.86. Although observations have shown that increased play between rail and joint bars leads to a lower joint efficiency factor, no quantitative method was available to determine its value.

On the other hand, both analytical models and field data were available to estimate the dynamic wheel load as a function of train speed for bolted joints. Jenkins, et al [4] developed an analytical model in which the dynamic wheel load is proportional to the impact velocity of the wheel running onto the receiving rail. The velocity is obtained from the "dip" angle at the joint that results from elastic and plastic deformation of the rail ends, Figure 2-2.

Experimental values of the effect of speed on wheel load for the bolted joint, provided by Ahlbeck, et al [5], show a roughly linear increase in load with speed consistent with the Jenkins, et al model.

These calculations and observations suggest that a model based on initial impact velocity provides a means of calculating the simultaneous effects of train speed and joint bar looseness on the bolt hole shear force.

In the discussion that follows, we will focus on the positive shear force at the first bolt hole. A shear force with this sign drives a crack that grows up and away from the rail end, which is the most commonly observed bolt hole crack.

FIGURE 2-2. DEFINITION OF DIP ANGLE USED BY JENKINS, ET AL [4]

2.2 APPROACH

A series of finite element analyses was performed in order to assess the effects of various parameters on bolt hole crack driving force through its correlation with rail shear force. A set of static calculations was performed in order to determine the effects of joint looseness on the shear force produced by the weight of the train. These calculations were made using a model which simulated the contact conditions between the rail and the joint bars. The model includes provisions for initial (static) and dynamic rail end height mismatch, but rail end gap·is not modeled. A set of dynamic calculations was then performed in order to determine the response of the rail end/joint/foundation system to impact from the vehicle unsprung mass and, in particular, to determine the dynamic contribution to the rail shear force.

The finite element code ABAQUS, Version 4.9 was used to perform both the static and the dynamic calculations. This commercially-available, general purpose finite element program is particularly well suited to solution of nonlinear problems.

2.3 STATIC CALCULATIONS

The rolling of the train wheel over the rail imparts a static load, P_0, to the rail due to the weight of the train. In this section, we discuss calculations aimed at determining the shear force in the rail at the location of the first bolt hole, V_b, and how this shear force changes when the joint becomes loose.

2.3.1 Model Description

A model consisting of a series of beam and gap elements was chosen as a simple, yet effective means of simulating the behavior of the rail and joint within the confines of a two-dimensional analysis. A schematic of the finite element model is shown in Figure 2-3. The rail was modeled using 1000 linear beam elements with nodes equally spaced at 0.0625 inch intervals between x=-25 inches and x=+25 inches (x=0 is the joint center) and nodes spaced at intervals varying from 0.0625 inches at x=±25 inches to 5.0 inches at x=±500 inches. The 36 inch joint bar was modeled using 576 beam elements with nodes also spaced at 0.0625 inch intervals. Beam section properties, and geometric properties for the rail and joint bar are summarized in Table 2-1 for the two cases studied: 100 lb/yd and 132 lb/yd rails with a 6-hole joint. The relatively light 100 lb/yd rail and the moderately heavy 132 lb/yd rail were chosen to provide estimates of response for the range of rail sizes currently in use.
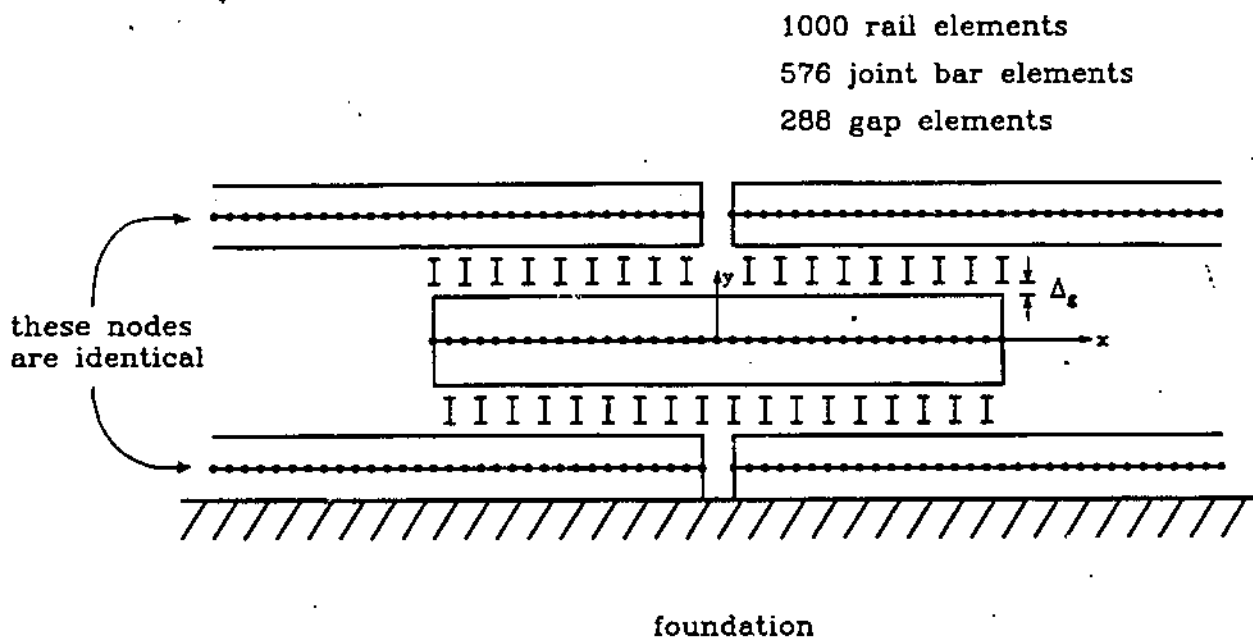
1000 rail elements

576 joint bar elements

288 gap elements

these nodes
are identical

foundation

FIGURE 2-3. **SCHEMATIC OF THE FINITE ELEMENT MESH USED FOR THE BOLTED JOINT**

TABLE 2-1.   SECTION PROPERTIES OF 100 AND 132 LB/YD RAIL AND JOINT BAR SETS

Rail Size	Component	Area (in^2)	Moment of Inertia (in^4)
100 lb/yd	Rail	10.0	49.0
	Joint Bar Set (2 bars)	10.1	17.9
132 lb/yd	Rail	12.9	88.2
	Joint Bar Set (2 bars)	11.0	28.7

The interaction of the rail and the joint bar was modeled using one-dimensional gap elements, oriented vertically, connecting rail and joint bar nodes located at equivalent x-axis positions. Gap elements are defined such that a force is transmitted across the gap if the difference between the vertical displacements of the two gap nodes exceeds a prescribed value, Δ_g. The gap elements can be oriented in two ways. In one orientation, the gap is defined such that a force is transmitted when the vertical displacement of the joint bar node exceeds that of the rail node by a distance Δ_g, thus simulating the interaction between the top of the joint bar and the underside of the rail head. In the opposite orientation, a force is transmitted when the vertical displacement of the rail exceeds that of the joint bar by the prescribed gap distance, simulating contact between the underside of the joint bar and the top of the base of the rail.   The model utilizes 288 gap elements - 144 in each direction - spaced at 0.125 inch intervals with alternating orientations.

In reference to Figure 2-3, we note that the rail nodes are shown as if they are positioned in both the upper and lower rail flanges of the rail. They are shown this way only to illustrate the contact that can occur between the rail nodes and the joint bar nodes. There is in reality only a single rail node at each x-axis position which occupies the same position as the corresponding joint bar node. The geometry of contact is controlled strictly through the vertical displacement of the rail and the joint bar and the interaction of the two through the gap elements.

The foundation was modeled as continuous using the FOUNDATION feature of ABAQUS, which automatically provides a springlike connection between each rail node and ground. A foundation modulus $u = 3000$ lb/in^2 was used.

The wheel load was modeled as a vertical concentrated force on the rail with magnitude $P_0 = 33,000$ lb.

Prior to analysis of the joint, a 132 lb/yd continuous rail subjected to a vertical load at the origin of magnitude P_0 was

2-6

modeled in order to validate the beam model. The calculated moment, $M_0=357,000$ in-lb, and vertical displacement, $\Delta_y=0.129$ inches, at the origin were compared with the classic analytical results (c.f. [6]) and found to differ by 0.5% and 1.6%, respectively. These results were taken as assurance that the use of beam elements was appropriate for modeling a beam-on-elastic foundation and that the model was properly defined.

Finite element calculations were carried out for each rail size with model gap sizes ranging from 0.0 to 0.030 inches and with load P_0 applied at various locations along the x-axis.

2.3.2   Results

The variation of the shear force at the first bolt hole (x = 3.5 inches) with wheel load position is shown in Figure 2-4 for gap sizes of 0, 0.001 and 0.010 inches for 132 lb/yd rail. The character of the 0-gap curve is in excellent agreement with results obtained in an earlier analysis using analytical models and also with strain gauge measurements [1]. For this case, the shear reaches a peak value of 32,200 lb when the wheel load is directly over the bolt; this compares to a maximum shear force of 16,500 lb that would be obtained for a continuous rail. The variation of the shear at the first bolt becomes somewhat more complex as the joint loosens, as is evident in Figure 2-4. When the gap size is 0.001 inches, the variation in shear still closely resembles that of the 0-gap case. More importantly, the peak shear for this case is actually greater (35,800 lb) than for the 0-gap case. For the much larger gap size of 0.010 inches, the shear distribution changes dramatically, indicating a change in contact conditions between the rail and the joint bar. The peak shear force for this case has decreased. Interestingly, the alternating shear force, which determines fatigue initiation conditions, has increased.

The bolt hole shear force/wheel load position curve becomes more complex with increasing Δ_g because of the changing distribution of gap forces. Figure 2-5 shows how this distribution changes as the gap size increases from zero to 0.010 inches for a wheel load at x = 3.5 inches. We note that the distribution becomes more discontinuous as the gap size increases, consistent with the discontinuous character of Figure 2-4.

The variation of shear force at the first bolt hole with joint looseness (gap size) from these calculations is plotted in Figure 2-6 for both 100 and 132 lb/yd rail. This plot shows that the maximum shear is slightly higher for the lighter rail, which is likely due to the higher joint efficiency factor (discussed below) for 100 lb/yd rail.

The joint efficiency factor, k, is a parameter that is commonly associated with degradation of rail end joints and so its calculation is included here for completeness. It is defined such that $k=M/M_0$, where M is the moment in the joint bars at the center of the bolted joint and M_0, as indicated earlier, is the moment
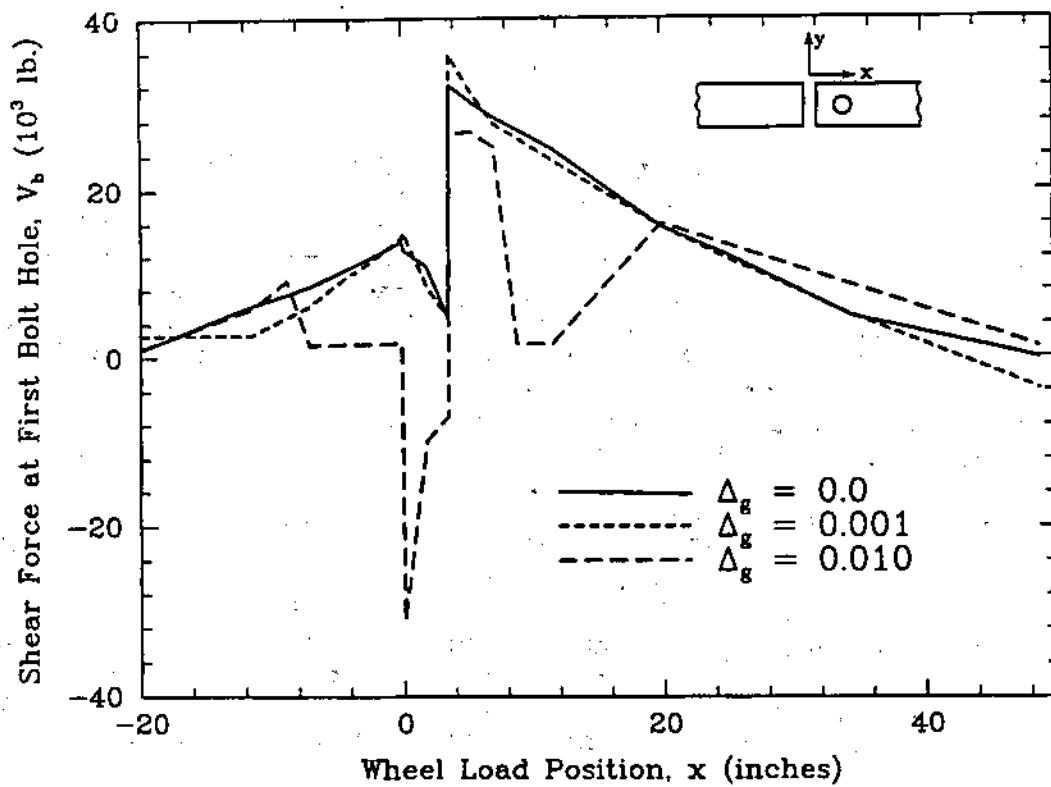
FIGURE 2-4. THE EFFECT OF RAIL/JOINT BAR GAP SIZE ON THE RAIL SHEAR FORCE AT THE FIRST BOLT HOLE (STATIC ANALYSIS)

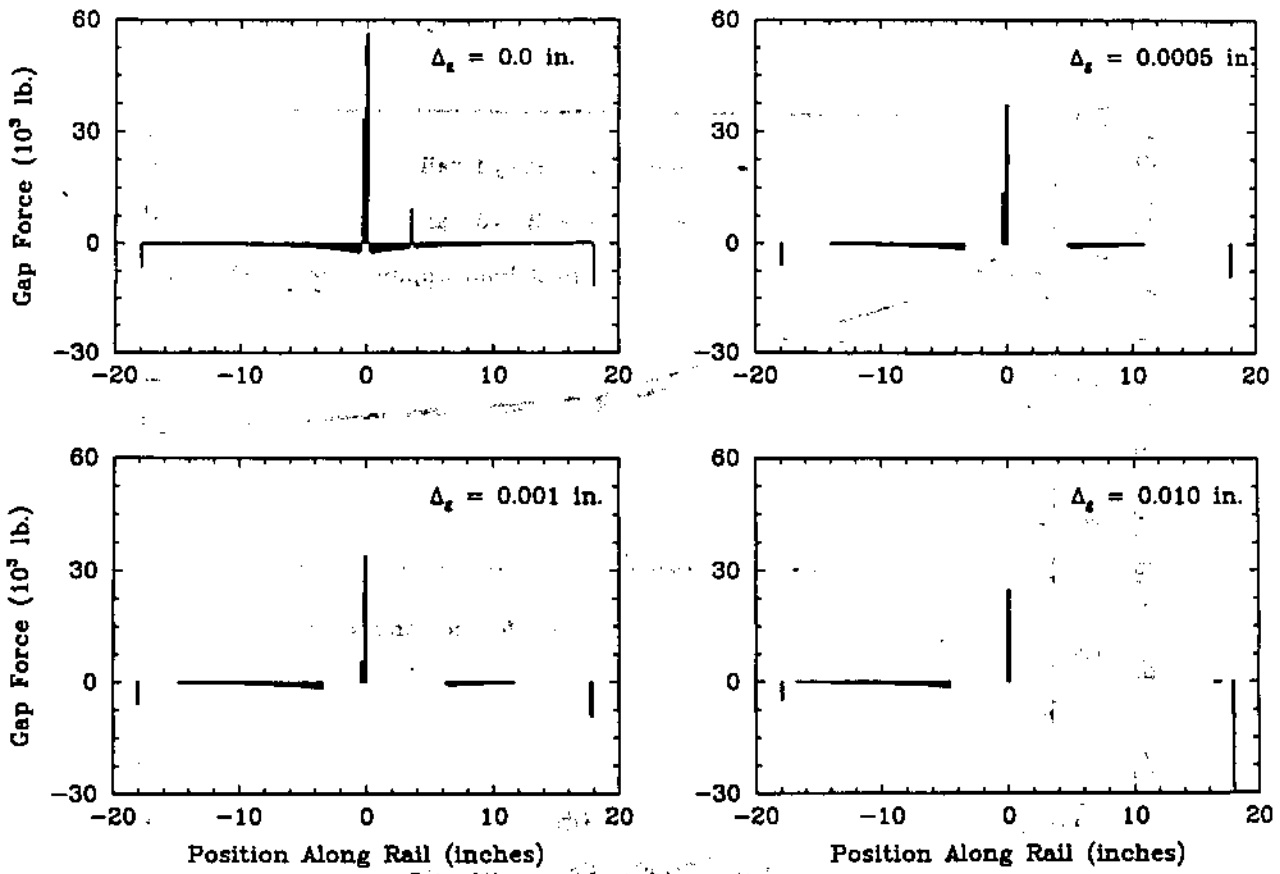**FIGURE 2-5. VARIATION OF THE CONTACT FORCE DITRIBUTION ALONG THE JOINT BAR WITH INITIAL GAP SIZE, Δ_g; WHEEL LOAD AT x=3.5 INCHES**
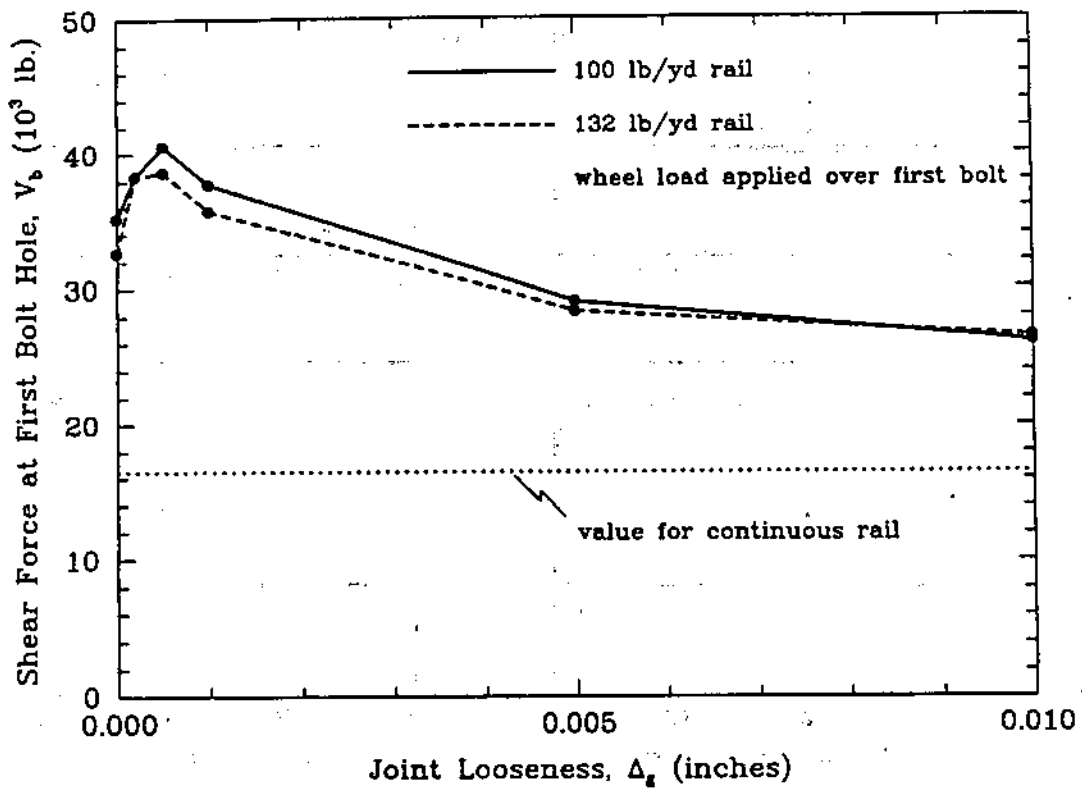
FIGURE 2-6.   THE MAXIMUM RAIL SHEAR FORCE AT THE FIRST BOLT HOLE
AS A FUNCTION OF GAP SIZE FOR TWO RAIL SIZES

that would occur at this same location if the rail were continuous. The parameter k was calculated for both rail sizes, for several gap sizes up to 0.030 inches, and for two loading conditions: one in which the load was applied at the rail end of the rail containing the bolt hole and one in which the load was applied over the first bolt hole (3.5 inches from the rail end). Calculated values of k are plotted versus gap size .for the two loading conditions in Figure 2-7. For 132 lb/yd rail, a maximum value of k=0.86 occurs when the gap size is zero; that is, when the rail and the joint bar are in contact along the entire length of the bar. As might be expected, k then gradually decreases with increasing gap size, reaching k=0.60 for a gap of 0.030 inches. The position of the wheel load does not seem to greatly affect k. The variation of k with gap size and load position is essentially the same for 100 lb/yd rail.

2.4 DYNAMIC CALCULATIONS

The motion of the vehicle over a rail end joint generates dynamic wheel loads that can be much greater than static loads. There are two major components to the dynamic loads imparted by impact of the wheel and the joint. The first component is a high frequency load associated with local Hertzian contact between the wheel and the rail. The dynamics associated with this system produces the so-called P_1 load (c.f.[4]). The second component is a lower frequency response associated with bending of the rail and compression of the foundation due to impact from the vehicle unsprung mass (the wheelset). The dynamics of this lower frequency system produces the so-called P_2 load, which is believed to be a strong determinant of the extent of fatigue cracking at the bolt holes through its correlation with the shear force at these holes. The P_2 load therefore has often been used as a measure of the extent of impact loading. One major benefit of using finite element methods, of course, is that bolt hole shear forces can be calculated directly from the analysis.

Efforts in this area were therefore directed at using finite element techniques to provide estimates of P_2 and, more importantly, V_b under various impact conditions. In particular, we studied the effects of joint bar looseness, train speed and rail height mismatch. The additional complexities inherent to dynamic analysis precluded the direct modeling of the joint bar/rail contact and joint looseness. We instead utilized results from the static analysis that enabled joint looseness to be indirectly taken into account, as will be described later in this section.
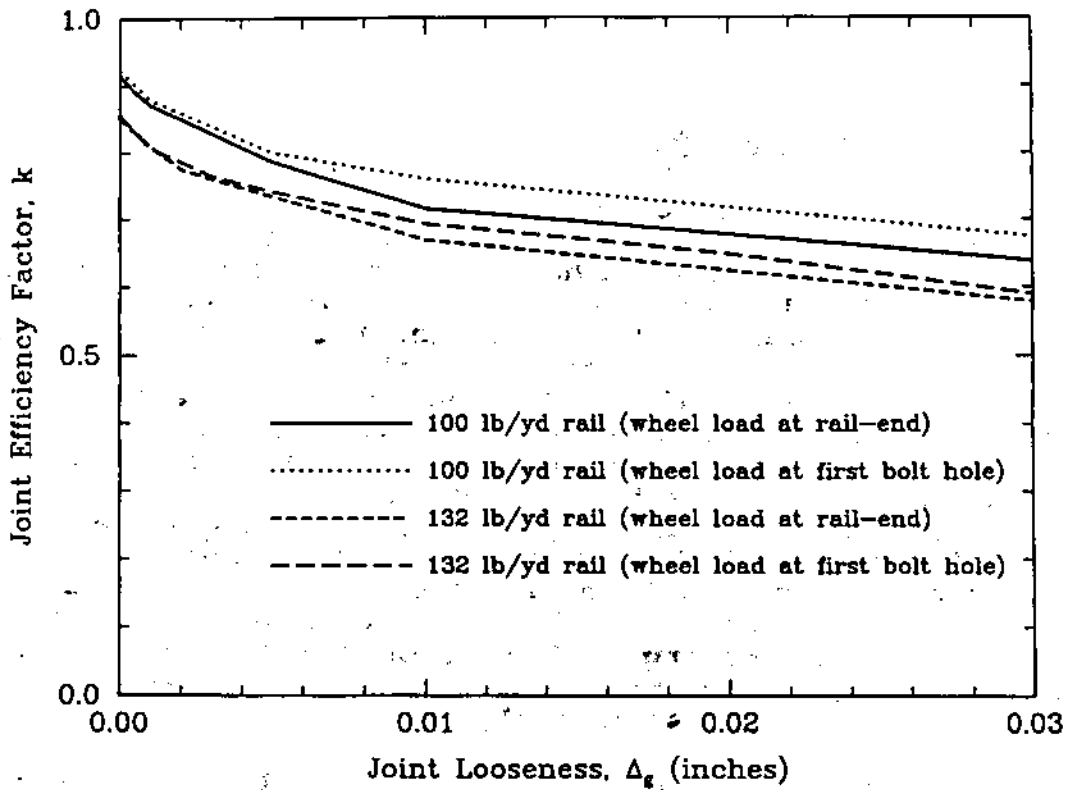
FIGURE 2-7. THE JOINT EFFICIENCY FACTOR AS A FUNCTION OF GAP SIZE FOR TWO RAIL SIZES AND TWO WHEEL LOCATIONS

2.4.1   Model Description

We used the MODAL DYNAMIC procedure of the ABAQUS finite element code for our dynamic calculations. With the MODAL DYNAMIC procedure, only a specified number of system modes and natural frequencies are calculated; the responses of the system to each mode are then linearly superposed to determine the total system response. The MODAL DYNAMIC procedure was chosen for use over the DYNAMIC procedure, in which the complete system response is directly calculated, in order to reduce model complexity and computation time. For a linear system, the results obtained using the MODAL DYNAMIC procedure become equivalent to those produced using the DYNAMIC procedure when the number of modes specified is equal to the number of degrees of freedom of the discretized system.   The beam impact modeling capabilities of ABAQUS are verified in Appendix A.

The basic approach taken to calculate the total shear force V_b at the bolt hole of interest was to sum the contributions to this force from: (1) the dynamic impact of the wheel with the rail end and; (2) the static wheel load; that is

$$V_b = V_b(dyn.) + V_b(stat.).$$

The procedure for calculating the dynamic component of V_b or P_2 was the following:

a.   Determine the nodes at which contact occurs between rail and joint bars for the degree of looseness under consideration using a static analysis with the wheel load located at the end of the rail onto which the wheel is crossing (the receiving rail).

b.   Fix these nodes in the subsequent dynamic calculations.

c.   Determine the initial velocity of the unsprung mass for the particular case at hand (described below) and use this value in the analysis to calculate $P_2(dyn.)$ or $V_b(dyn.)$.

The contribution to P_2 or V_b from the dynamic impact event is determined by calculating the response of the rail to an impulse forcing function that depends on the initial velocity v_o of the unsprung mass, m. The value of v_o will depend on train speed and the degree to which there is mismatch in slope and height at the rail ends, and must first be calculated for the various cases analyzed. Procedures described in the previous section are used to calculate the static wheel load contribution, which depends on wheel load location and also the degree of joint bar looseness. We note that the peak value of the sum of these two contributions will not always correspond to the peak values of each individual contribution, due to the importance of wheel load location and its dependence on train speed and time.

A different finite element mesh was designed to model the dynamic response of the rail end/joint system. It consisted of 100 linear beam elements for the rail and 73 linear beam elements for the joint bar. Within the joint region, the rail and joint bar nodes occupied identical x-axis positions, spaced at 0.5 inch intervals. Except where noted, each corresponding pair of rail/joint bar nodes was pinned together, so that their displacements were equal, simulating rail/joint bar contact.

Following Goldsmith [7], the impact boundary conditions were modeled by introducing the following time-dependent load at the impact node:

$$P(t) = 2mv_0\pi/\tau \sin(\pi t/\tau) \quad 0 < t < \tau$$

$$= 0 \quad t > \tau ,$$

where m and v_0 are the mass and transverse (vertical) velocity of the wheelset, and τ is the duration of contact, which can be determined by solving the Hertzian contact problem. We did not attempt to calculate τ. Our calculations showed, however, that as long as τ is much less than the period of the first natural mode of the rail end/joint bar/foundation system the results are independent of τ.
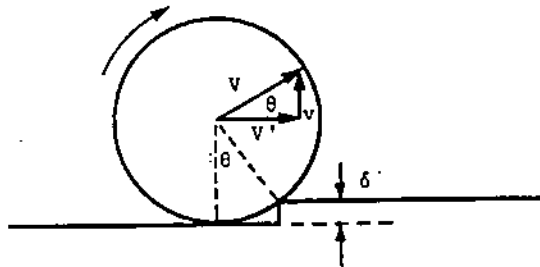
2.4.2   Results

The case of a rail end height mismatch will serve to illustrate the method for calculating v_0 as well as a means to determine the proper number of modes for use in these dynamic calculations. Following the procedure of reference [8], illustrated in Figure 2-8,

$$v_o = [2\delta/R]^{1/2}V \tag{1}$$

where δ = rail height mismatch,
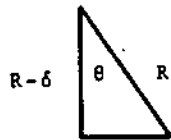   R = wheel radius,
         V = train speed.

A calculation of the peak force, P_2, was made for comparison to the analytical results in [8]. The parameters used were: u = 4,000 lb/in^2; P_0 = 33,000 lb; R = 20 inches; I_r = 88.2 in^4 (132 lb/yd rail); m = 2000 lb; V = 10 mph and; δ = 0.18 inches. All rail/joint bar contact nodes were fixed for the rail height mismatch calculations.

This provides a transverse impact velocity v_0=23.61 in/sec. Finite element calculations of contact point acceleration, which is proportional to the dynamic wheel load, P_2(dyn.), for this model problem are shown in Figure 2-9 for 1-mode, 6-mode, 10-mode, and 20-mode solutions.   The 1-mode solution provides a direct comparison with the single degree-of-freedom analytical results of the noted report. Our calculated natural frequency f=35 Hz is in reasonable agreement with the analytical estimate of f=40 Hz. (Some differences between analytical and numerical results should be expected, due to differences between the calculated stiffness of

$$v = V \sin \theta$$
$$V' = V \cos \theta$$

$$\cos \theta = \frac{R-\delta}{R} = (1 - \frac{\delta}{R})$$

$$\sin \theta = \sqrt{1 - (1 - \frac{\delta}{R})^2} \simeq \sqrt{2 \frac{\delta}{R}} \quad \text{for small } \frac{\delta}{R}$$

$$v = \sqrt{2 \frac{\delta}{R}} \ V$$

$$V' = (1 - \frac{\delta}{R}) \ V$$

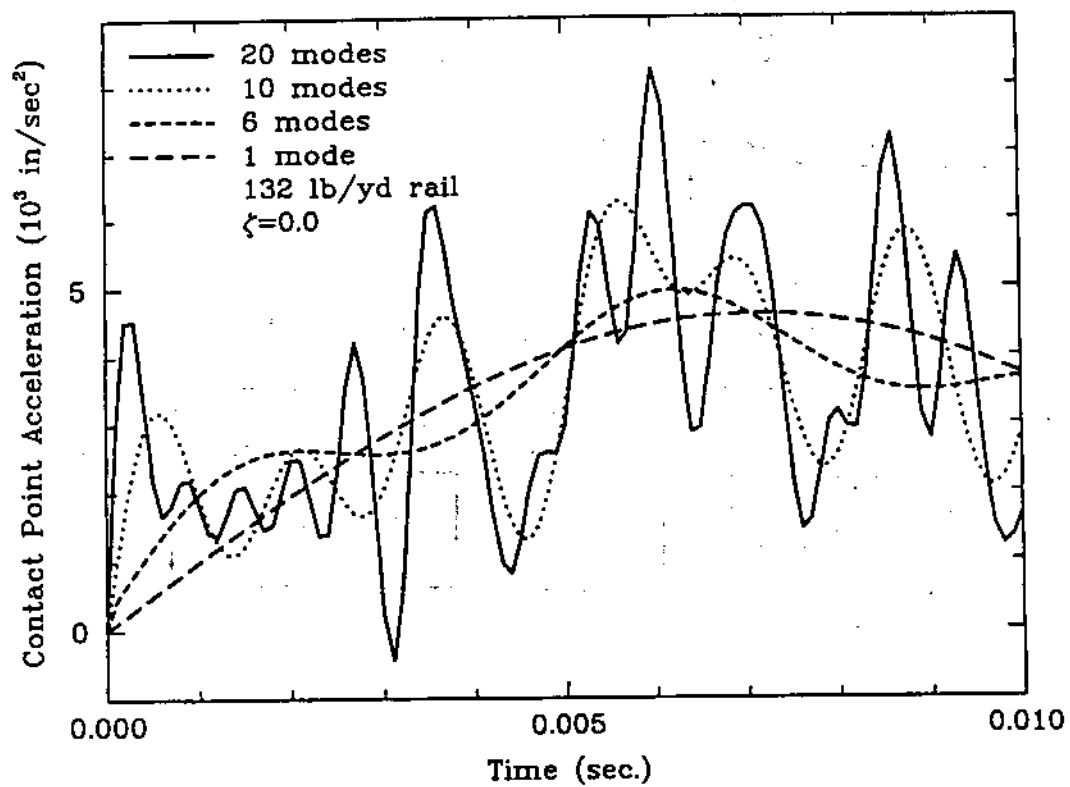**FIGURE 2-8.   AN ILLUSTRATION OF THE METHOD USED TO CALCULATE WHEEL IMPACT VELOCITY (FROM [8])**

FIGURE 2-9. WHEEL CONTACT POINT ACCELERATIONS FOR VARIOUS NUMBERS OF DYNAMIC MODES; NO DAMPING CASE

the numerically-modeled system, and the assumed stiffness $k_s = 3.3 \times 10^5$ used in the analytical model. A static analysis using the numerical model yields an equivalent system stiffness of $k_s = 2.8 \times 10^5$ for a load equal to P_0 applied at the rail end.)

It is clear from the data depicted in Figure 2-9, that higher mode terms contribute to the response as well. However, much of the higher frequency response will be damped out for actual rail conditions. Calculations were made using two values of damping [9]: a standard value, $\zeta = 0.30$, and a reduced value, $\zeta = 0.10$, where $\zeta = 0.433[c_f^2/um_t]^{1/2}$, c_f = foundation damping coefficient and m_t = track mass. An example of the calculated contact acceleration made using $\zeta = 0.10$, shown in Figure 2-10, demonstrates that much of the higher order contribution to system response dies out even when this reduced damping is added.

Table 2-2 summarizes calculated values of P_2/P_0 for several cases analyzed; P_2 is the sum of the product of the contact acceleration and the unsprung weight, m = 2000 lb, and the static wheel load. Without damping, the 20-mode solution provides a prediction that is 33% higher than the 1-mode prediction and 15% higher than the 10-mode prediction. With 10% damping, the 20-mode solution is only 5% higher than the 1-mode solution and only 0.1% higher than the 10-mode solution. Finally, With 30% damping, the 20-mode and 10-mode solutions are virtually identical, and are only 1% higher than the 1-mode solution. Based upon these results, we believe that 10 modes are sufficient to capture the dynamic response for $\zeta = 0.10$ or greater.

Figure 2-11 summarizes the shear force response at the rail end for the model problem using the 10-mode solution. The maximum shear force decreases as damping increases.

Confident that the finite element method is providing good predictions of rail-impact loads, we proceeded to evaluate the consequences of other rail height mismatch values: $\delta = 0.25$ inches and 0.5 inches. All other parameters were the same as for the previous rail height mismatch analysis except, u = 3000 lb/in². The transverse velocity component from equation (1) is $v_0 = 27.8$ and 41.2 in/sec for $\delta = 0.25$ and 0.5 inches, respectively. For the idealized joint of Figure 2-8, the 0.5 inch height mismatch produces a contact position about 4.4 inches from the rail end for the running off case. The smaller mismatch of 0.25 inches produces a contact point only 3.1 inches from the rail-end. This difference is potentially significant because the primary point of interest - the first bolt hole - is 3.5 inch from the rail-end, so the contact points for the two cases are on opposite sides of the bolt hole.

The results of calculations for P_2 and the dynamic contribution to V_b are summarized in Table 2-3. These solutions are linear so we can generate a curve showing the variation of the dynamic component bolt hole shear force with train speed for each of the two cases (Figure 2-12).
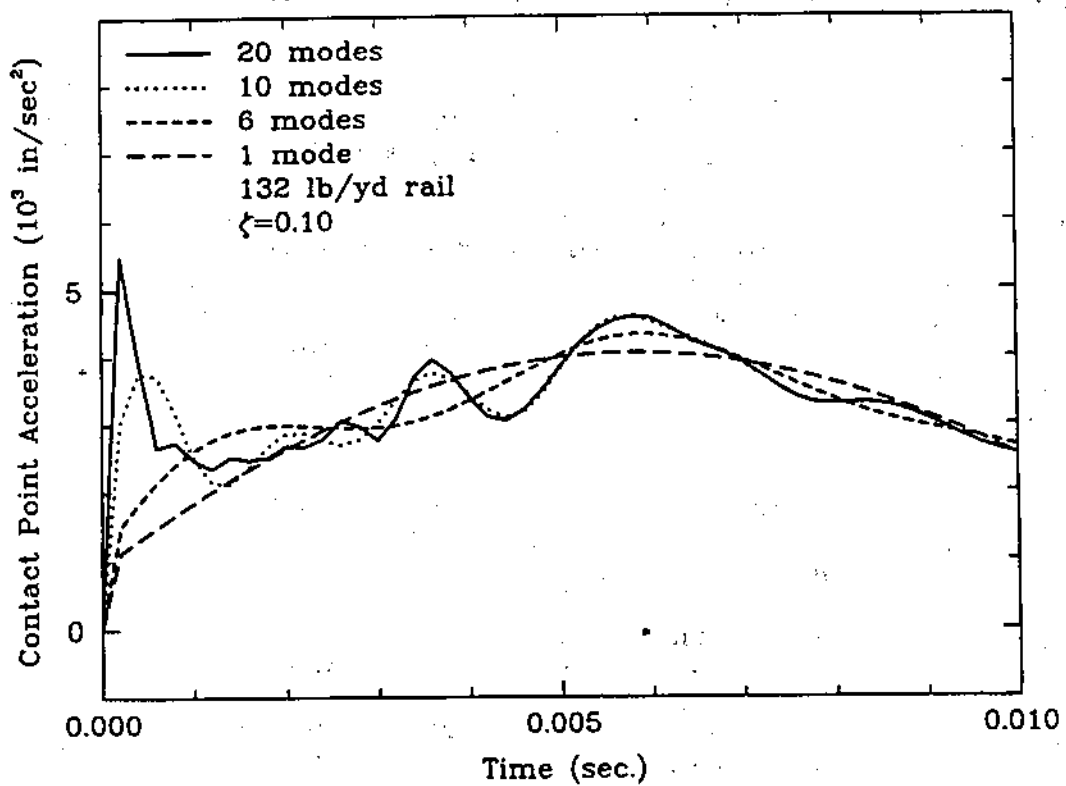
FIGURE 2-10. WHEEL CONTACT POINT ACCELERATIONS FOR VARIOUS NUMBERS OF DYNAMIC MODES; DAMPING CASE

TABLE 2-2.   A COMPARISON OF FINITE ELEMENT PREDICTIONS OF P_2 FOR DIFFERENT NUMBERS OF MODES USED, WITH AND WITHOUT DAMPING

Number of Modes	P_2/P_0		
	$\zeta=0$	$\zeta=0.10$	$\zeta=0.30$
1	1.724	1.636	1.588
6	1.775	1.679	1.556
10	1.985	1.720	1.572
20	2.290	1.722	1.572
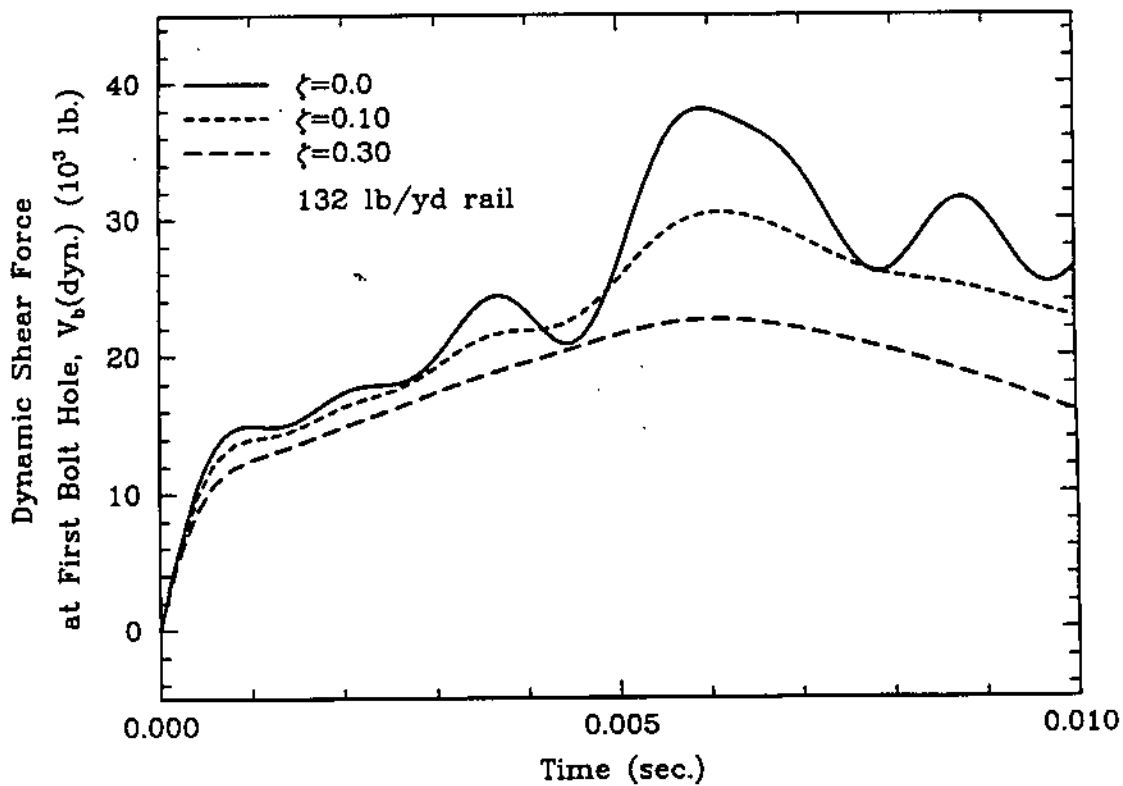
FIGURE 2-11.   DYNAMIC RAIL SHEAR FORCE AT THE FIRST BOLT HOLE FOR VARIOUS DEGREES OF DAMPING

TABLE 2-3. FINITE ELEMENT MODEL ESTIMATES OF P_2/P_0 AND $V_b(DYN.)/P_0$ FOR 0.25 INCH AND 0.5 INCH RAIL-HEIGHT MISMATCHES ; $\zeta = 0.10$; 10 MPH.

Rail-Height Mismatch (inches)	P_2/P_0	$V_b(dyn.)/P_0$
0.25	1.865	0.715
0.50	2.065	0.961

FIGURE 2-12. DYNAMIC RAIL SHEAR FORCE AT THE FIRST BOLT HOLE AS A FUNCITON OF TRAIN SPEED AND RAIL END HEIGHT MISMATCH

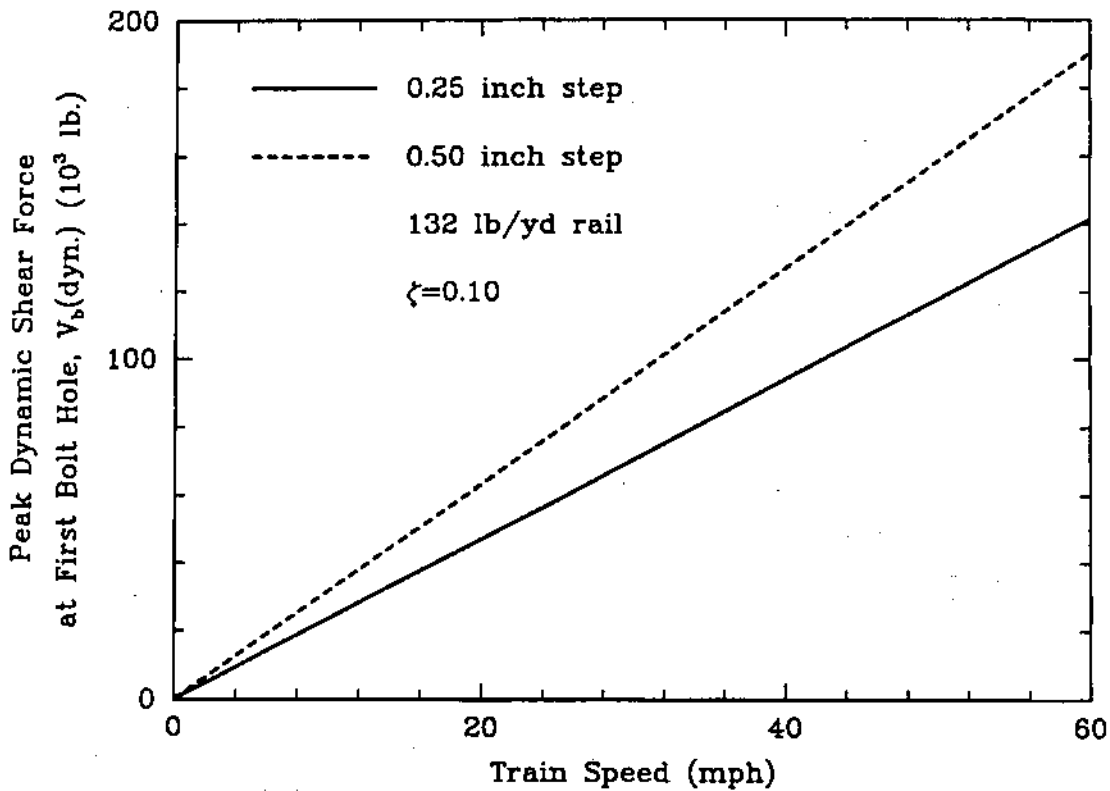In order to estimate the total shear force at the first bolt hole, we must sum its static and dynamic contributions. The peak in static bolt hole shear force depends upon the position of the wheel when the peak dynamic load occurs. We can estimate the total shear force at the bolt by transforming the dynamic shear force versus time data into shear force versus wheel position data using the assumed impact location and the speed of the train. We can then superpose these data with those obtained in the static analysis (Figure 2-4). The results of this superposition are shown in Figure 2-13 and indicate that, for a train speed of 10 mph, the maximum bolt hole shear force is equal to 55,100 lb for a 0.25 inch mismatch and increases to 61,600 lb for a 0.5 inch mismatch. We note that, in these cases, the peak total shear force coincides in time with the peak dynamic shear force and very nearly with the peak static shear force.

If train speed is increased the peak dynamic response will occur when the wheel is further down the rail so that the dynamic contribution to the maximum total shear force at the first bolt will not increase proportionally, but by a somewhat reduced factor. Likewise, if the step size is further increased, the impact velocity will increase by the square root of this factor, but the impact location will move further away from the first bolt, so that the dynamic part of the total shear force will increase by somewhat less than the square root factor. For the two cases presented here, an increase in step size of a factor of two resulted in an increase in the dynamic contribution to the maximum total shear force by a factor equal to 1.34.

We next considered the effects of joint looseness on dynamic response. Figure 2-14 shows the vertical displacement of the rail near the rail end that we determined in the static analysis for 100 lb/yd rail and for several gap sizes. As one might expect, the displacements increase as the gap size or joint looseness increases. In addition, a mismatch between the vertical displacements of the opposing rail ends arises and becomes much more prominent as joint looseness increases.

As noted earlier in this report, when there is no mismatch, Jenkins et al [4] suggested that the transverse component of velocity, v_0, is approximately equal to the sum of the joint dip angles multiplied by the train velocity. An additional component of transverse velocity due to the rail end displacement mismatch can be estimated using the methods outlined in Figure 2-8. For this case, an estimate of the step height, δ, was taken to be equal to the vertical displacement of the wheel as it moves from a position in which the wheel load is balanced upon both rail ends to one in which the entire load is transmitted to one rail end. This step height was calculated by subtracting the balanced wheel load displacement profile from the displacement profile shown in Figure 2-14 (see Figure 2-15). A conservative estimate of the total transverse velocity was then made by assuming that the dip angles
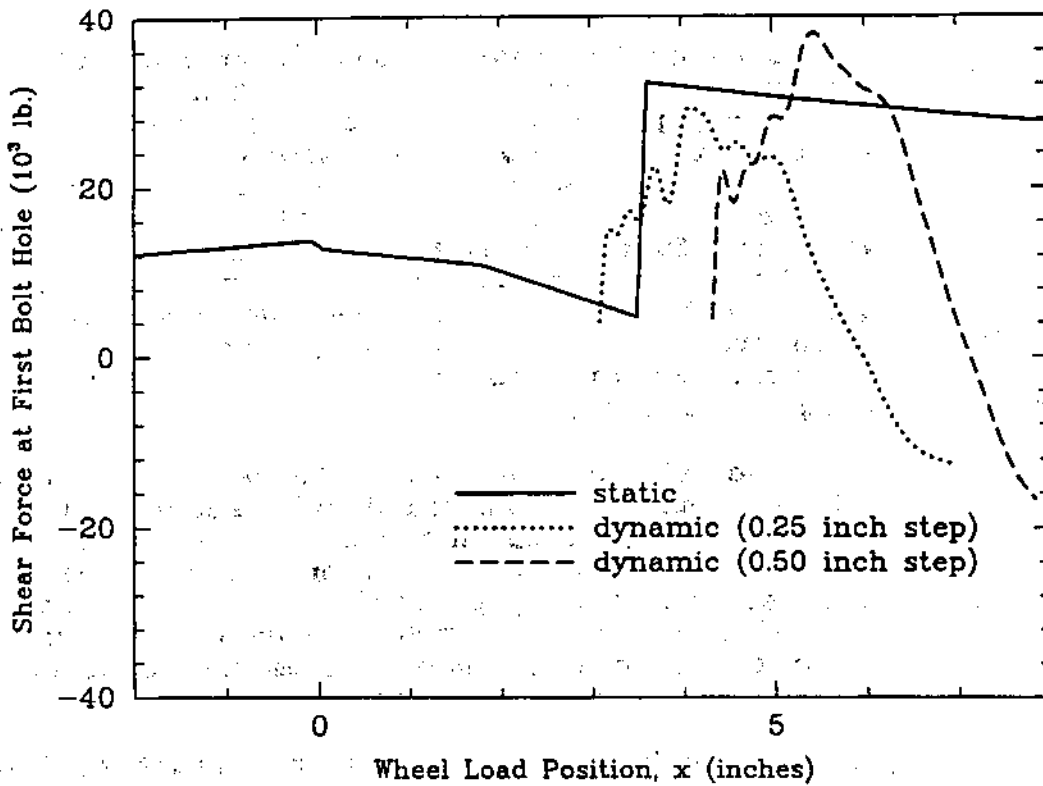
FIGURE 2-13. STATIC AND DYNAMIC RAIL SHEAR FORCES AT THE FIRST BOLT HOLE AS A FUNCTION OF WHEEL LOCATION
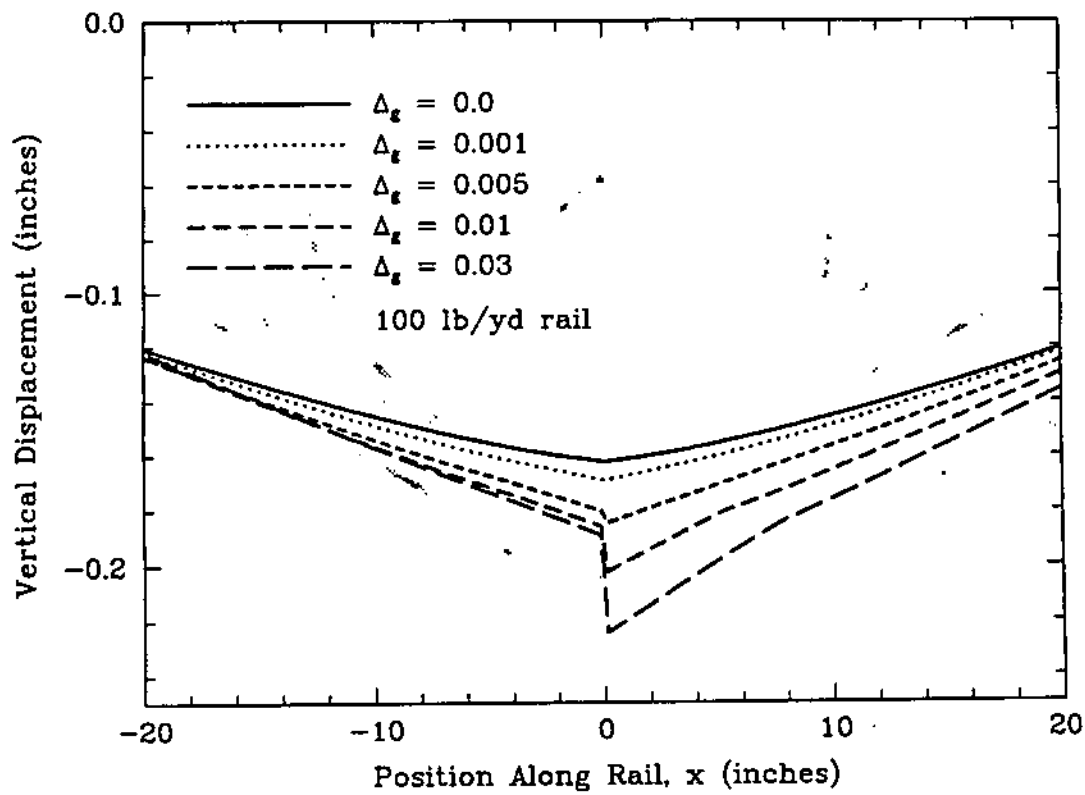
FIGURE 2-14. RAIL VERTICAL DISPLACEMENT NEAR THE JOINT FOR
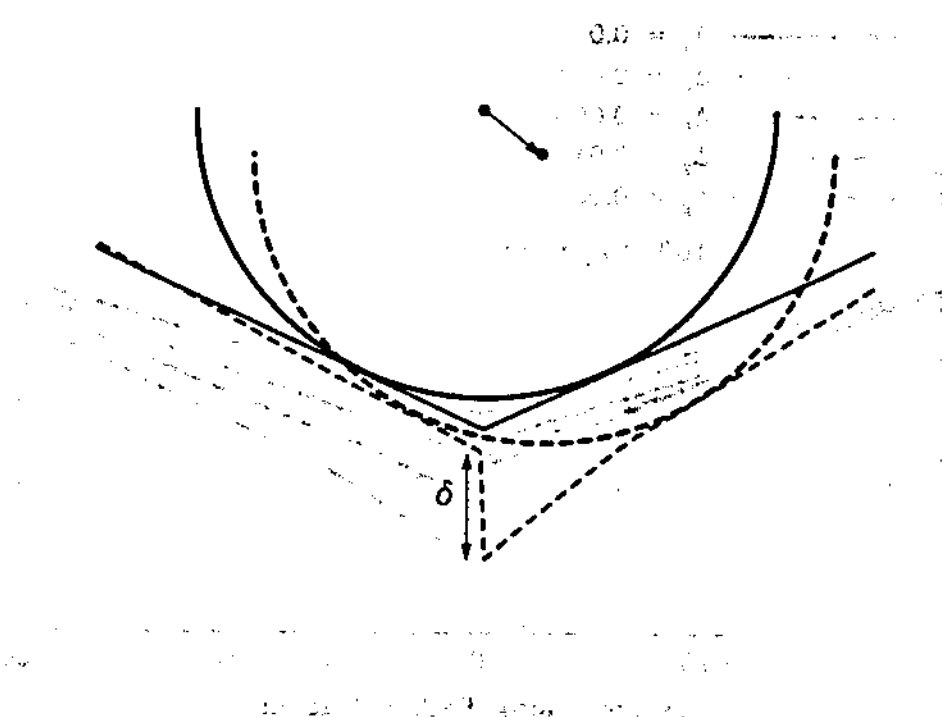VARIOUS INITIAL GAP SIZES

2-23

FIGURE 2-15. ILLUSTRATION OF THE METHOD USED TO CALCULATE IMPACT
VELOCITY FOR THE LOOSE JOINT CASE

have no effect on the calculations of the displacement mismatch and then summing the two velocity contributions, so that

$$V_0 = (\alpha_1 + \alpha_2 + \sqrt{2}\delta/R)V,$$

where α_1 and α_2 are the dip angles on the trailing and leading edge of the rail, respectively.

The calculated dip angles, displacement mismatches and vertical velocities for several gap sizes are shown in Table 2-4. The static solutions for 100 lb/yd rail with an applied rail end load were used to calculate these values. The resulting impact calculations are summarized in Table 2-5 for a train speed 60 mph. Since these solutions are linear, they can be scaled to other train speeds. The large increase in rail end displacement mismatch coupled with the change in rail/joint bar contact conditions causes large increases in P_2 and V_b(dyn.) with joint looseness increases up to 0.010 inches. In particular, there is a dramatic increase in both P_2 and V_b(dyn.) when the joint looseness increases from 0.005 inches to 0.010 inches, which is primarily due to the substantial increase in rail end displacement mismatch and the associated increase in impact velocity.

TABLE 2-4.   EFFECT OF JOINT LOOSENESS ON a_1, a_2, δ, AND V_0 (V=60 MPH)

Joint Looseness (inches)	α_1	α_2	δ (inches)	V_0 (in/sec) (V=60 mph)
0.000	0.0012	0.0012	0.0000	2.5
0.001	0.0020	0.0020	0.0007	13.1
0.005	0.0032	0.0030	0.0029	24.5
0.010	0.0048	0.0033	0.0203	56.1
0.020	0.0055	0.0035	0.0310	68.3
0.030	0.0061	0.0036	0.0425	79.1

TABLE 2-5. **EFFECT OF JOINT LOOSENESS ON $V_b(DYN.)/P_0$ AND P^2/P_0 FOR V=60 MPH**

Joint Looseness (inches)	$V_b(dyn.)/P_0$	P_2/P_0
0.000	0.02	0.07
0.001	0.22	0.34
0.005	0.25	0.61
0.010	0.52	1.43
0.020	0.30	1.73
0.03	0.14	1.98

At joint looseness values greater than Δ_g=0.010 inches, the rate of increase in the impact velocity becomes much smaller, as does the resulting rate of increase in P_2. At the same time, however, the loss of contact between the rail and the joint bar becomes more widespread, causing the system stiffness to decrease, and redistributing the applied load. The net result is a decrease in values of V_b(dyn.) with a positive sign that is, a sign that causes a crack to grow up and away from the rail end.

A conservative estimate of the total bolt hole shear force can be made by summing V_b(dyn.) with the value for V_b(stat.) calculated when the wheel load is directly over the first bolt hole. The contributions of each to the total bolt hole shear force is plotted as a function of joint looseness in Figure 2-16 for a 60 mph train speed. This curve shows that the total, positive shear force at the first bolt hole also increases when the joint becomes loose, and then decreases as the degree of joint looseness becomes large.

It should be noted that the method employed for this analysis - using the static solutions to calculate the impact velocities and rail/joint bar contact conditions - provides only an approximation to actual dynamic contact conditions. The severe loss of contact associated with the larger gap sizes ($\Delta_g \geq 0.010$) causes the mechanics of contact to become quite complex. Our calculations indicated that for these large gap sizes, the calculated contact conditions could be sensitive to the position of the applied static load.

When introduced into the dynamic model, with its much fewer degrees of freedom, we found that these changes in the contact conditions could have significant effects on the predictions of V_b(dyn.). Given the general complexity of the problem and the uncertainty in predicting the actual contact location, and given that the results of the numerical analysis suggests that a small change in joint looseness can have a significant effect on the shear force at the
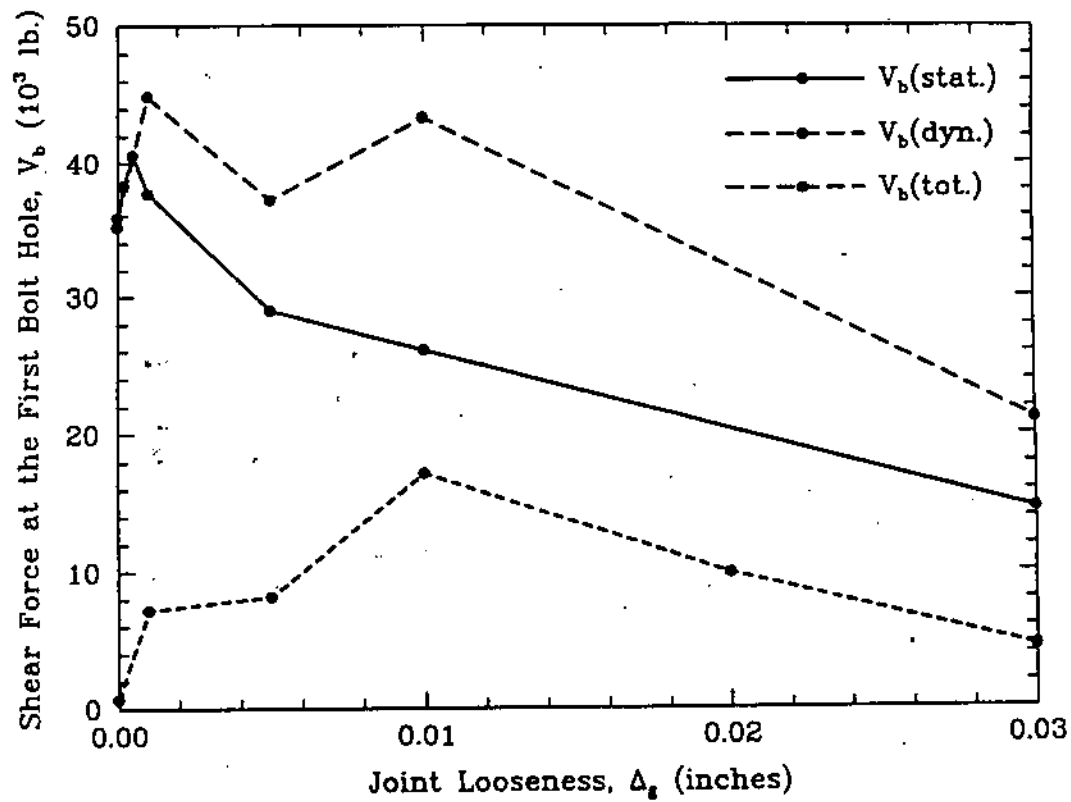
FIGURE 2-16.   STATIC, DYNAMIC AND TOTAL RAIL SHEAR FORCE AT THE FIRST BOLT HOLE AS A FUNCTION OF INITIAL GAP SIZE FOR 132 LB/YD RAIL, 60 MPH TRAIN SPEED

bolt hole of interest, we feel that the predictions of V_b(total) for the large gap sizes must be viewed with some degree of uncertainty.

2.5 DISCUSSION

The two-dimensional beam model of the bolted joint provides a physical basis for relating the crack driving force to joint bar looseness. The results show that under static conditions the maximum shear force at the first bolt hole decreases with increasing gap size between bar and rail. In fact, a reduction occurs in this force of 20% in going from a tight joint to one with a gap of only 0.010 inches. However, associated with this reduction is a greater contribution from the dynamic load, caused by the increasing discontinuity in slope and height at the joint. Figure 2-16 shows each contribution and their sum for a particular set of conditions. We infer from this figure that the defect is at greater risk of fracture when the joint is loose consistent with general field experience.

The magnitudes of the predicted shear forces can be examined to determine whether fracture is actually predicted for any particular case. Previous experimental work showed that a Mode I stress intensity of approximately 25 ksi$\sqrt{}$in is obtained for a positive bolt hole shear force of 50,000 lb in 136 lb/yd rail. We will also use this relationship for 132 lb/yd rail. Measured fracture toughness of plain carbon rail steel can vary from K_c = 25 to 50 ksi$\sqrt{}$in. Using data from Figure 2-16, from which V_b(max) = 45,000 lb, and the relationship between shear force and stress intensity, we see that the predicted maximum value of K_I is 22.5 ksi$\sqrt{}$in for a 60 mph train speed. Thus, it appears that there is a risk of fracture for these conditions if the joint has become loose and the material toughness is low. The presence of thermal or residual stresses would also increase the risk of fracture.

It is at first surprising that the predicted shear force at the first bolt hole does not increase monotonically with joint bar gap size, especially since dynamic wheel load, P_2, increases steadily with Δ_g.

This phenomenon is due to the change in contact conditions at the rail end. As the joint bar loosens, the upward acting (positive) contact forces decrease between the rail end and the first bolt hole. Consequently, the downward acting wheel load begins to exert the dominant influence on the shear force at the first bolt hole. In the absence of joint bars, this force would be almost entirely negative. These results indicate that a crack oriented up and toward the rail end, rather than the oppositely oriented most common bolt hole crack, will be much more likely to fracture as the joint bars continue to loosen.

The dynamic finite element analysis also provides data with which to evaluate the effect of a rail end height mismatch. A value of 0.25 inches is currently allowed for Class 1 track (limited to 10 mph). The model developed in this study predicts that the bolt hole shear force would increase by only 10% in going from a 0.25 to 0.50 inches. Such a small increase would not seem to be of concern except that the bolt hole shear force magnitudes they produce are relatively high: 55,100 and 61,600 lb. The estimated maximum stress intensities for these values are $K_I = 27.6$ and 30.8 ksi$\sqrt{in}$. Thus, some demonstration of safety with high reliability at 0.25 inches would seem necessary before increasing the allowable height to 0.50 inches.

3. VERTICAL SPLIT HEAD

3.1 PRIOR WORK

Nearly all of the research to date on the vertical split head has been directed at the determination of the conditions under which the defect occurs rather than predicting the rate of crack growth and the conditions under which complete fracture can occur [10-12].

The form of the vertical split head defect most often observed in service, after the rail has been removed and cross-sectioned, is shown in Figure 3-1. The crack consists of three segments: (1) the primary, vertical segment which can extend from the approximate area of the head-web fillet to within about 0.3 inches of the running surface; (2) an angled segment at the top of the head, whose tip can eventually intersect the running surface, and; (3) a bottom curved segment that approaches the head-web fillet surface, usually in a direction opposite the top, angled segment. A definitive correlation has not yet been made between the orientation of the upper, angled crack and the gage or field side of the rail during the last part of its service. Observations on the fracture surfaces of these cracks generally show that the vertical and lower curved segments consist of cleavage facets, while the upper angled segment exhibits the ductile features characteristic of fatigue crack growth.

Another interesting feature of the vertical split head cross section is the degree of crack opening at the intersection of the straight and top, angled segments. This characteristic is common in the defects we have observed and appears to be indicative of the prior existence of high, transverse tensile residual stress and accumulated plastic flow.

Vertical split head cracks can be quite long; we have examined one whose length was over seven feet. All of the defects we have examined were long relative to their vertical extent. The benefit of this high aspect ratio defect geometry in analysis is the ability to use a two-dimensional geometry model, even though the loading is still three-dimensional.

Prior work on the crack driving force for this defect was directed exclusively at the straight, vertical segment. Metallographic studies, finite element analyses and laboratory tests indicate that two conditions are required for the occurrence of a vertical split head: a zone of weak microstructure near the center of the rail head, and the accumulation of significant tensile residual stresses also at the center of the rail head. Under these conditions the weak microstructure acts as a precrack whose rapid growth initiates when the combined action of the residual stress and a live load induce a stress intensity that exceeds the local material toughness. Finite element analysis and laboratory tests show that
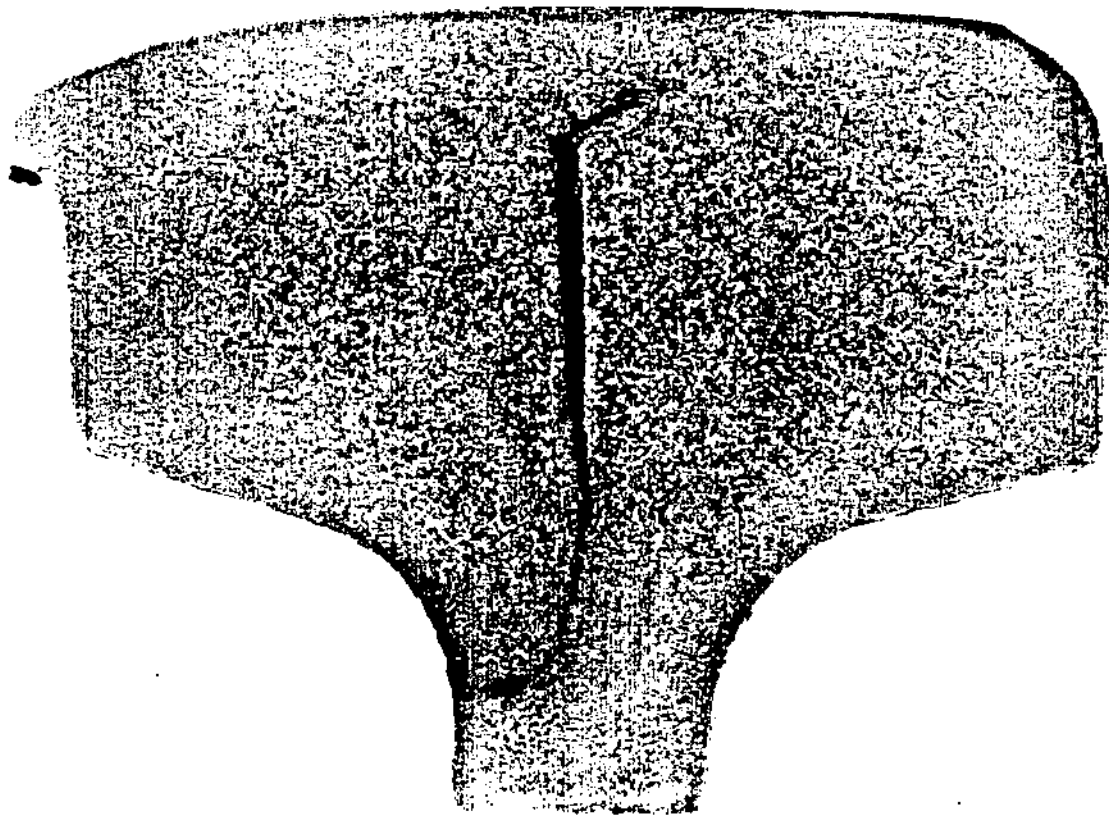
FIGURE 3-1.   A METALLOGRAPHIC   CROSS   SECTION   OF   A   TYPICAL
VERTICAL SPLIT HEAD DEFECT.

the stress intensity factor at the tip of the crack decreases with crack size, explaining why the defect usually arrests before intersecting a free surface. The compressive residual stresses at the running surface also assist in this arrest process. Metallographic examination and fracture toughness tests show that the defect length is determined by the extent of the weak microstructure as well.

Prior analysis provided only tentative explanations for the occurrence of the upper and lower angled segments of the vertical split head. Previous finite element analyses showed a substantial mixed mode loading component for a straight, vertical crack with an off-center loading. This suggested that loading at one of the rail head corners is the explanation for the top, angled crack. The angled portion at the head-web fillet is probably caused by a bending load or the presence of residual stresses.

Although little specific work on final fracture had been conducted, the great vertical extent of this defect together with the observation of plastic flow in the cross section suggest that final fracture is controlled by some plastic limit load process.

Some of the important conclusions of the prior work that relate to the present effort are summarized here:

- The initial vertical split head defect consists of a vertical segment whose upper tip is approximately 0.3-0.4 inches from the running surface.

- Vertical split heads are generally long relative to their vertical extent, with the greatest additional growth occurring in the vertical direction away from the axial ends of the defect.

- Additional, subcritical growth from an initial vertical split head appears to occur exclusively at the top crack tip.

- The top crack tip grows by fatigue at an angle of approximately 30° to a horizontal line.

3.2 APPROACH

Results from the prior work showed that an understanding of the crack growth behavior from the angled crack segment is necessary, because it is the most commonly observed shape.

Finite element analysis was used to calculate stress state and fracture mechanics parameters for a vertical split head that included this geometry. Less time-consuming two-dimensional analysis was used to establish the effects on crack driving force of wheel load location and top crack segment angle and three-dimensional analysis was used to determine stress intensity factors and stress distributions for realistic loading.

The cross-sectional geometry and mesh used for both types of analyses correspond to a 132 lb/yd rail and are shown in Figures 3-2a, 3-2b and 3-2c. The vertical split head crack consists of a straight, vertical segment, 1.3 inches in length, centered in the rail cross section, the bottom tip of which is located 1.65 inches below the running surface. The angled segment is 0.2 inches in length and oriented from 20 to 40° from the horizontal, depending on the calculation performed. The finite element program ABAQUS Version 4.9 was used for all calculations. Contact between crack faces is not modeled, which is consistent with the relatively large crack openings exhibited by these defects when in the unloaded state. All analyses were elastic with Young's modulus and Poisson's ratio 30×10^6 lb/in^2 and 0.3, respectively.

Stress intensity factors were calculated using the procedure of Matos, et al [13] in which the countour J-integral is combined with relative crack face displacements to determine K_I and K_{II}. Shown in Figure 3-2c are the coordinate systems local to each of the crack tips, which are important for determining the sign of the Mode II stress intensity factor; K_{II} is positive when the top face of the crack (+y) moves in the positive x-direction relative to the bottom face of the crack.

3.3 TWO-DIMENSIONAL CALCULATIONS

The objective of the two-dimensional finite element calculations was to select a specific crack angle and wheel loading location for the three-dimensional analyses. A line load of 10,000 lb/in was chosen arbitrarily and analyses were conducted using a plain strain idealization. The mesh shown in Figure 3-2b consisted of 256, eight node, biquadratic elements resulting in a total of 2,000 degrees of freedom. The base of the rail was constrained only from deflections in the vertical direction. The wheel was represented by a point load applied downward in the vertical direction at a node on the running surface.

Results of the calculations are shown in Figures 3-3 through 3-6. Figure 3-3 shows the Mode I stress intensity factor for the upper crack tip as a function of wheel load position for the three segment angles analyzed. These data show that the maximum, positive opening mode stress intensity occurs when the wheel load is at the extreme corner of the rail head, opposite the direction of the angled segment. The figure also shows that the angle of the upper segment, for the range of angles analyzed, has little effect on the magnitude of K_I. However, we note that the length of the angled segment was kept constant and not the distance to the running surface.

Figure 3-4 shows that the opening mode stress intensity at the lower crack tip is greatest when the load is approximately centered on the rail head. The magnitude of K_I is smaller than for the upper crack tip and there is no significant variation with crack angle. The Mode II stress intensity factor for the upper crack tip for an
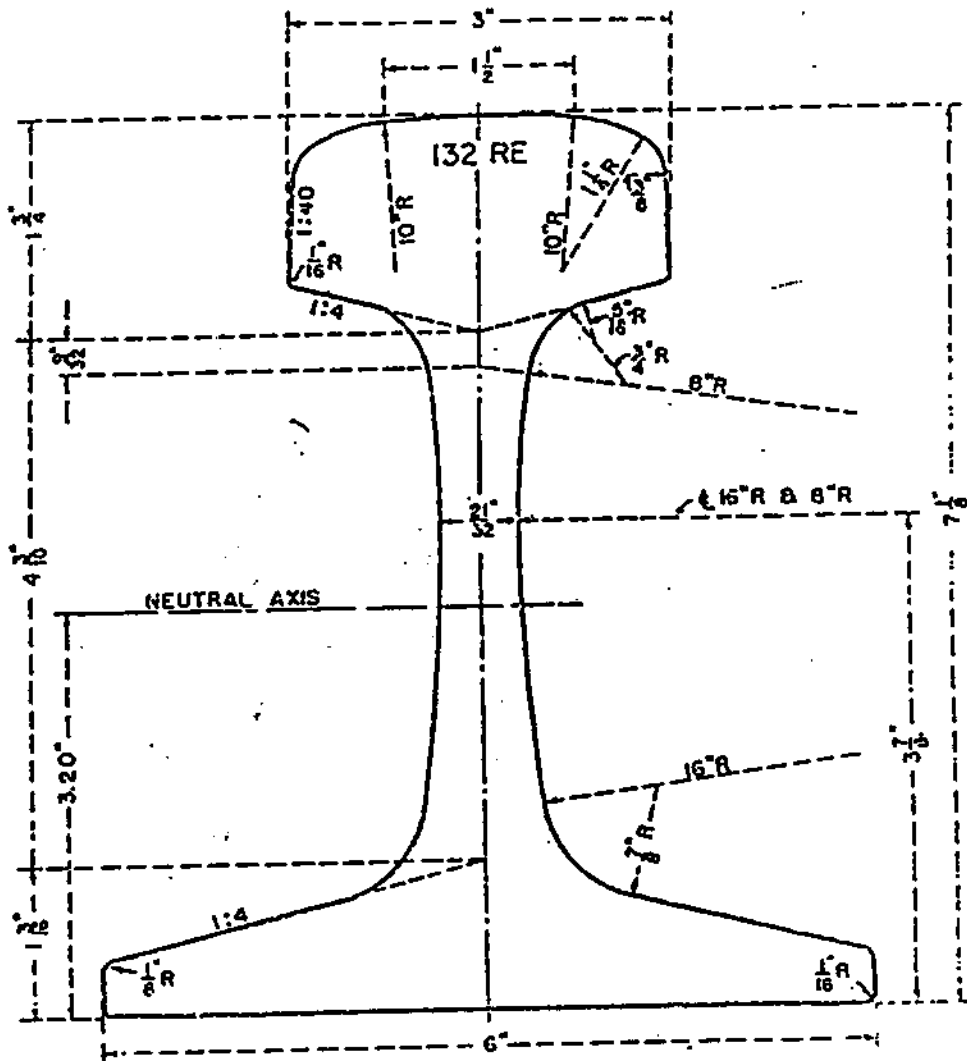
FIGURE 3-2(a). THE CROSS-SECTIONAL GEOMETRY USED FOR THE FINITE ELEMENT ANALYSIS: RAIL DIMENSIONS

ABAQUS

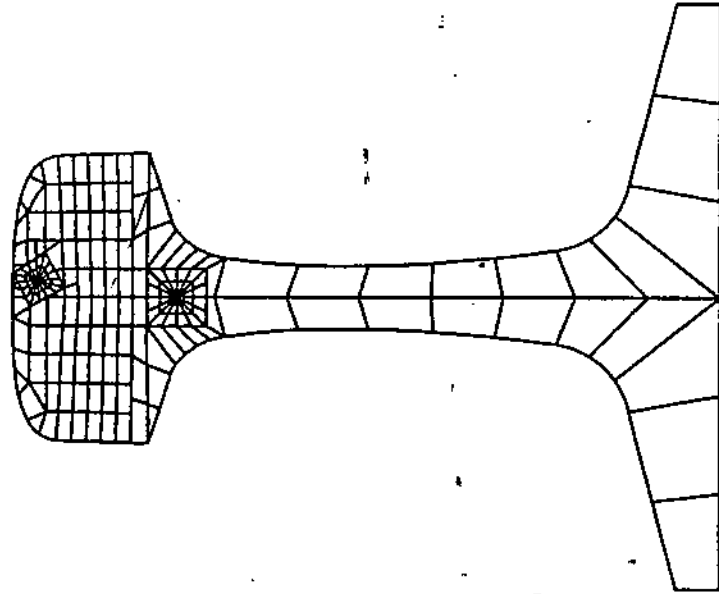FIGURE 3-2(b). THE CROSS-SECTIONAL GEOMETRY USED FOR THE FINITE ELEMENT ANALYSIS: MESH
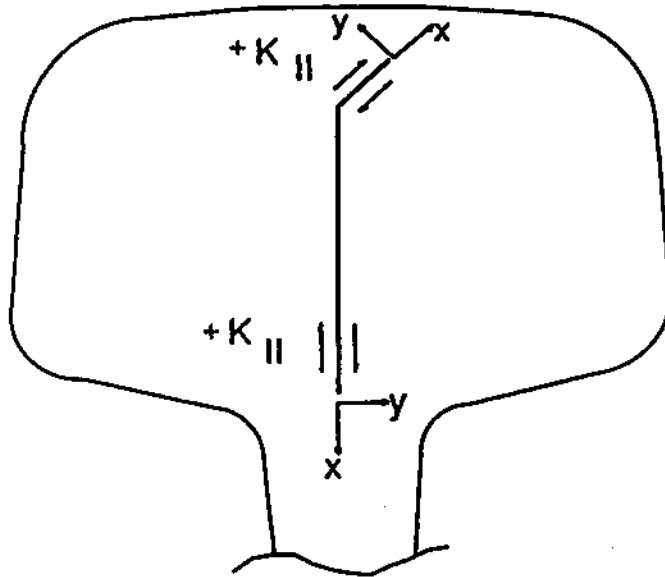
FIGURE 3-2(c). THE CROSS-SECTIONAL GEOMETRY USED FOR THE FINITE ELEMENT ANALYSIS: CRACK TIP COORDINATE SYSTEMS

FIGURE 3-3.　　MODE I STRESS INTENSITY VS. WHEEL POSITION FOR THE
UPPER CRACK TIP:　TWO-DIMENSIONAL ANALYSIS

FIGURE 3-4. MODE I STRESS INTENSITY VS. WHEEL POSITION FOR THE LOWER CRACK TIP: TWO-DIMENSIONAL ANALYSIS

FIGURE 3-5. MODE II STRESS INTENSITY VS. WHEEL POSITION FOR THE UPPER CRACK TIP: TWO-DIMENSIONAL ANALYSIS

FIGURE 3-6. MODE II STRESS INTENSITY VS. WHEEL POSITION FOR THE LOWER CRACK TIP: TWO-DIMENSIONAL ANALYSIS

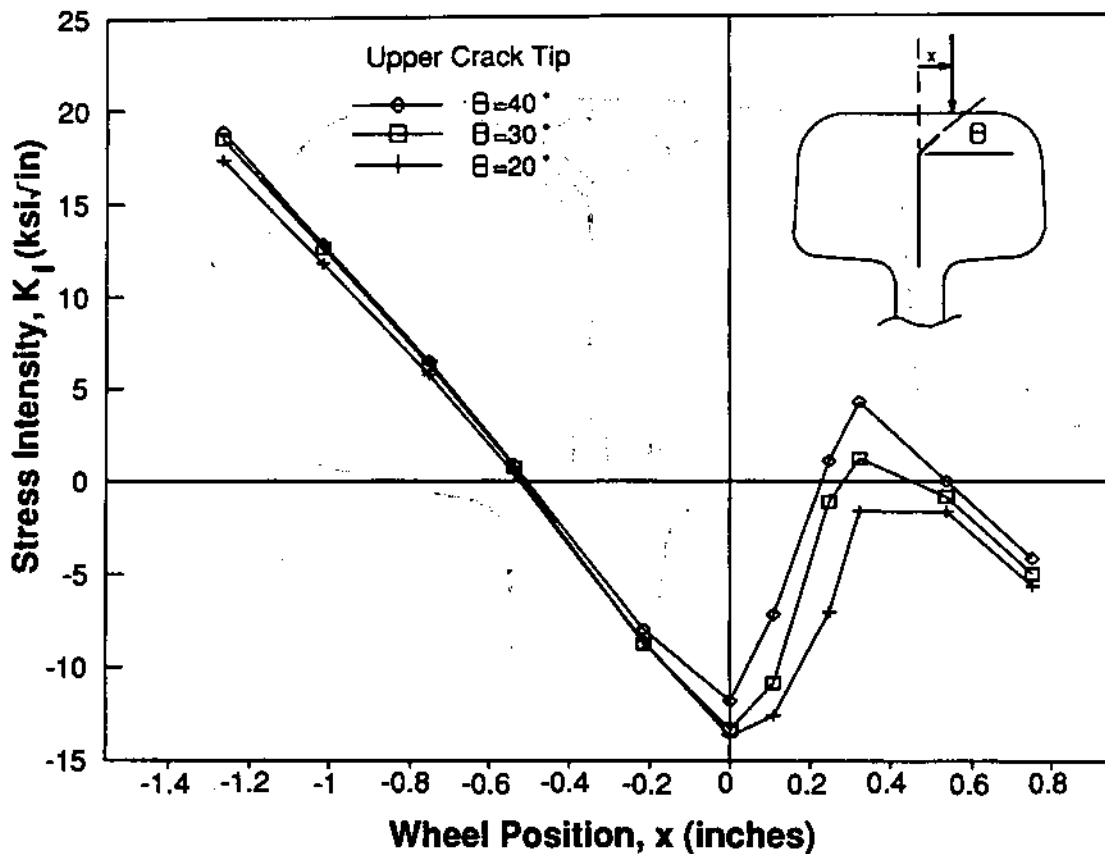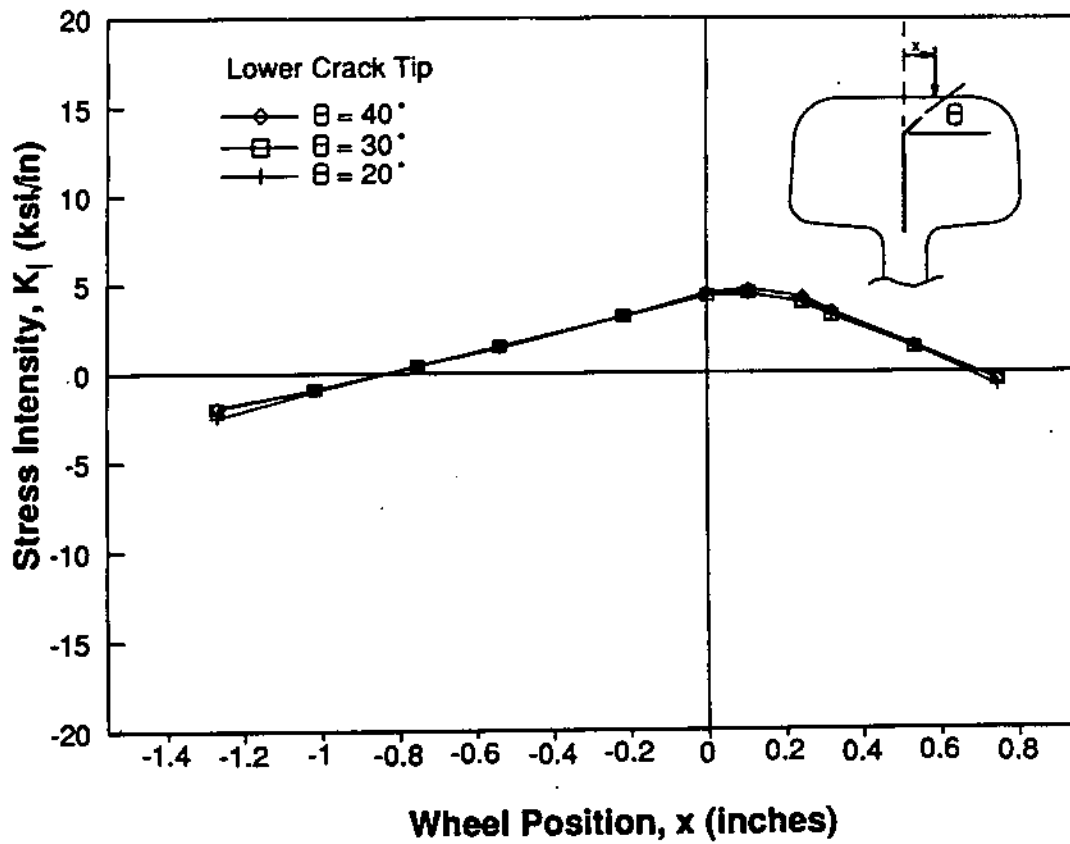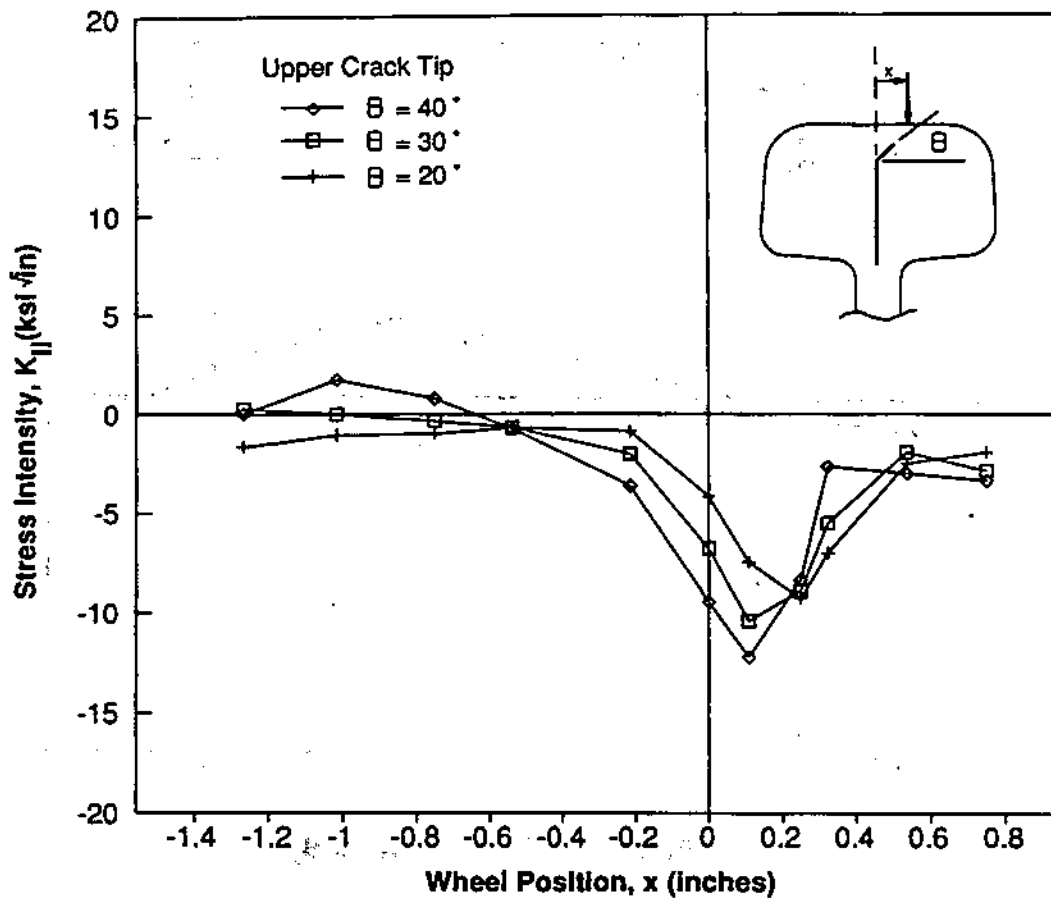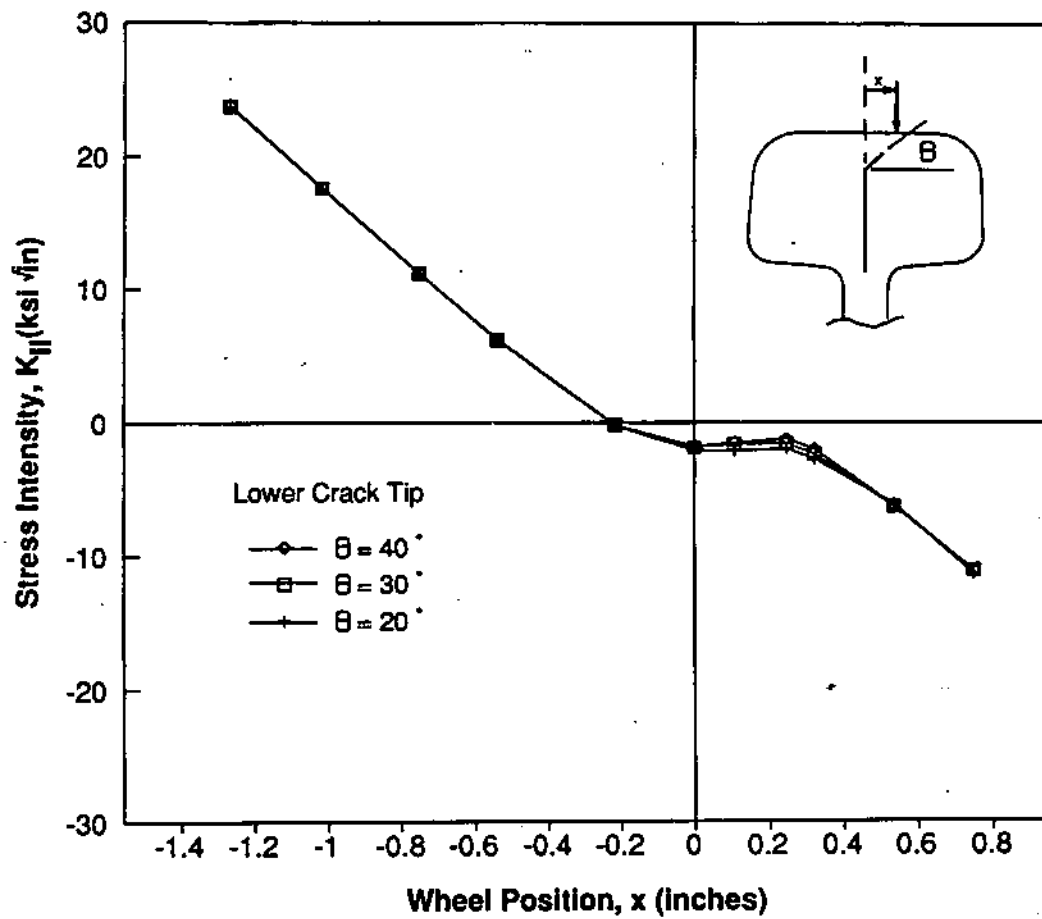upper segment angle of 30° is a minimum when the load is at the same location for which K_I is a maximum: the rail head corner opposite the direction of the angled segment, Figure 3-5. On the other hand, K_{II} is positive and a maximum at the lower crack tip for this configuration, Figure 3-6. A positive K_{II} tends to drive the lower crack tip toward the head-web fillet in a direction opposite the upper, angled crack segment, which is the same lower crack orientation observed in defects removed from service.

These results provide us with a number of useful conclusions about vertical split heads:

a. The stress intensity factors of interest for the upper and lower crack tips are not sensitive to the angle of the upper crack segment for the range of angles observed in service.

b. Defects in service are apparently subjected to wheel loads that are concentrated on the side of the rail head opposite the direction of the angled crack segment.

c. A load concentrated at this location also tends to drive the lower crack in a direction consistent with that observed in service.

3.4 THREE-DIMENSIONAL CALCULATIONS

Three-dimensional calculations are necessary to correctly model the loading applied to the vertical split head. Wheel loads in service are applied to the running surface over an elliptical area whose length along the rail is approximately 0.6 inches. On the other, hand, the head behaves as a beam on an elastic foundation - the web - resulting in the load being distributed over several inches at the head-web junction. This contrasts to the two-dimensional model which simulates equal line loads at the running surface and head-web junction.

The same cross-sectional mesh used for the two-dimensional calculations, Figure 3-2b, was used for the three-dimensional analyses. Only one upper segment angle, 30°, was analyzed. The length of the mesh in the third dimension was 6 inches because of computational constraints. Nine layers were used, Figure 3-7, the thicknesses of which increase in a geometric progression, beginning with 0.16 inches and ending with 1.6 inches. The entire mesh consisted of 1,340, 20-node, quadratic displacement brick elements resulting in a total of 35,800 degrees of freedom. All of the nodes on the planes at either end of the mesh were constrained in the axial direction, making both cross sections planes of symmetry. The vertical deflections at the base of the rail were also constrained. All loads were applied at the plane of symmetry corresponding to the thinnest layer of elements.
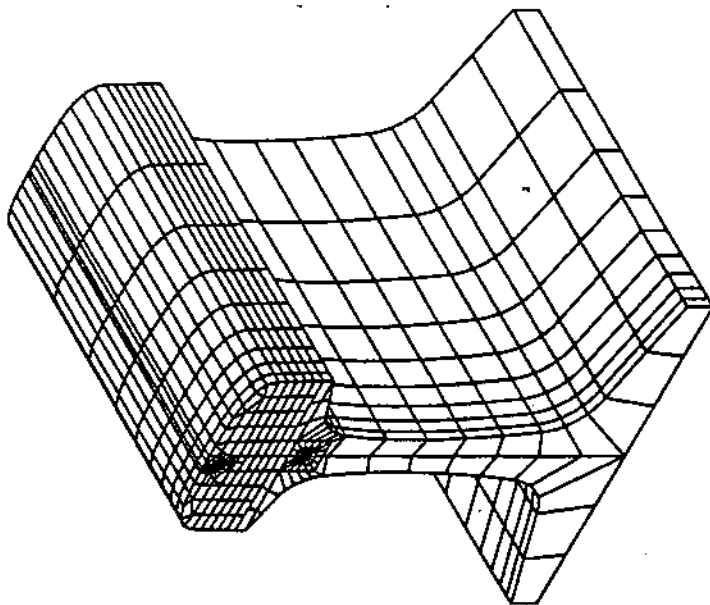
ABAQUS

FIGURE 3-7. THE THREE-DIMENSIONAL FINITE ELEMENT MESH

These boundary conditions essentially model an infinitely long rail with loads applied every 12 inches. In other words, the stress intensity factor, and all other stresses, determined at the location of load application will include a contribution from two other loads each 12 inches away (as well as contributions from more distant loads). At the time of the analysis, we felt that this model would provide the best boundary conditions for a short length rail model; prior work [12] indicated that the stress intensity factors were close to zero at locations 6 inches from the point of load application. As shown below, this assumption failed to be completely correct for the angled crack case.

A more limited set of loading conditions was analyzed in three dimensions. These included: (1) a vertical point load of 33,000 lb applied at the center of the running surface, directly over the vertical segment of the defect, and (2) a 33,000 vertical point load applied at a distance of 1.27 inches from the center, opposite the direction of the angled segment of the defect.

A plot of the Mode I and Mode II stress intensity factors for the upper crack tip as a function of distance from the centrally located point load is shown in Figure 3-8. These results are consistent with the two-dimensional results which show that the top crack tip experiences a high compressive stress intensity for the centrally located load. The ratios of K_{II}/K_I are also comparable for the two analyses: 0.34 (3-D), 0.50 (2-D). Figure 3-9 shows the results for the lower crack tip for this load case. Both of these figures show that the stress intensity becomes negligible at a distance of approximately 3 inches from the load.

The results for the more interesting rail head corner load case are shown in Figures 3-10 and 3-11. These results cannot be taken as even a good approximation to the stress intensity distribution for a single load, because of the relatively high values of K_I and K_{II} at the unloaded end of the rail model (x = 6 inches). However, some important information can be drawn from the figures. For example, it is reasonable to assume that the contribution to K_I and K_{II} at x = 6 inches is due primarily to the nearest loads, each located 6 inches away; the next nearest loads are 18 inches away. The actual stress intensity values at x = 6 inches should then be approximately one-half of those shown on the figures, or K_I = 2.1 ksi$\sqrt{}$in compared to a maximum value of about 7 ksi$\sqrt{}$in. This suggests that the contribution from a load 12 inches distant will not be very large. In fact, the form of the K_I distribution in Figure 3-10, which actually shows a maximum 1.5 inches from the plane of loading, suggests that the contributions from loads 12 inches away are small and negative. In summary, we believe that the top crack tip stress intensity values at the plane of loading for the model used are good approximations to the values that would be obtained for a single load on an infinite rail.

FIGURE 3-8. **MODES I AND II STRESS INTENSITY FACTORS FOR THE UPPER CRACK TIP: CENTRALLY LOCATED WHEEL LOAD**
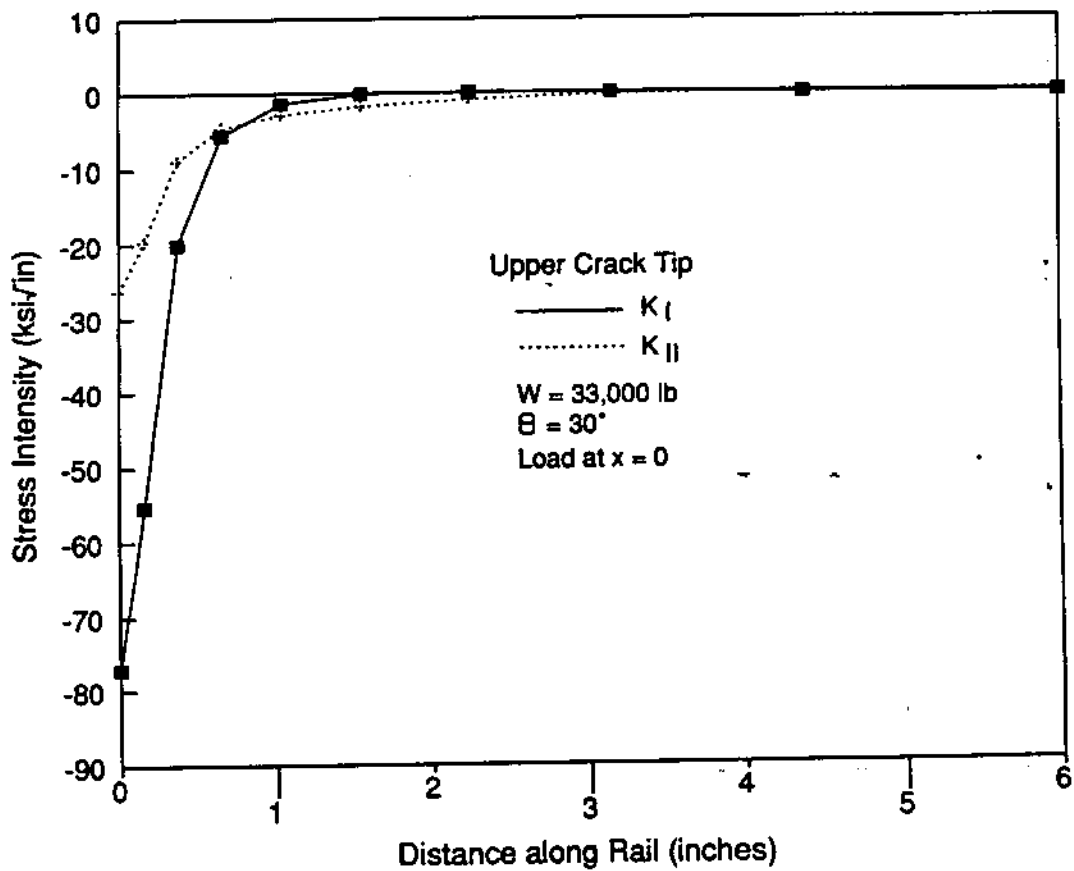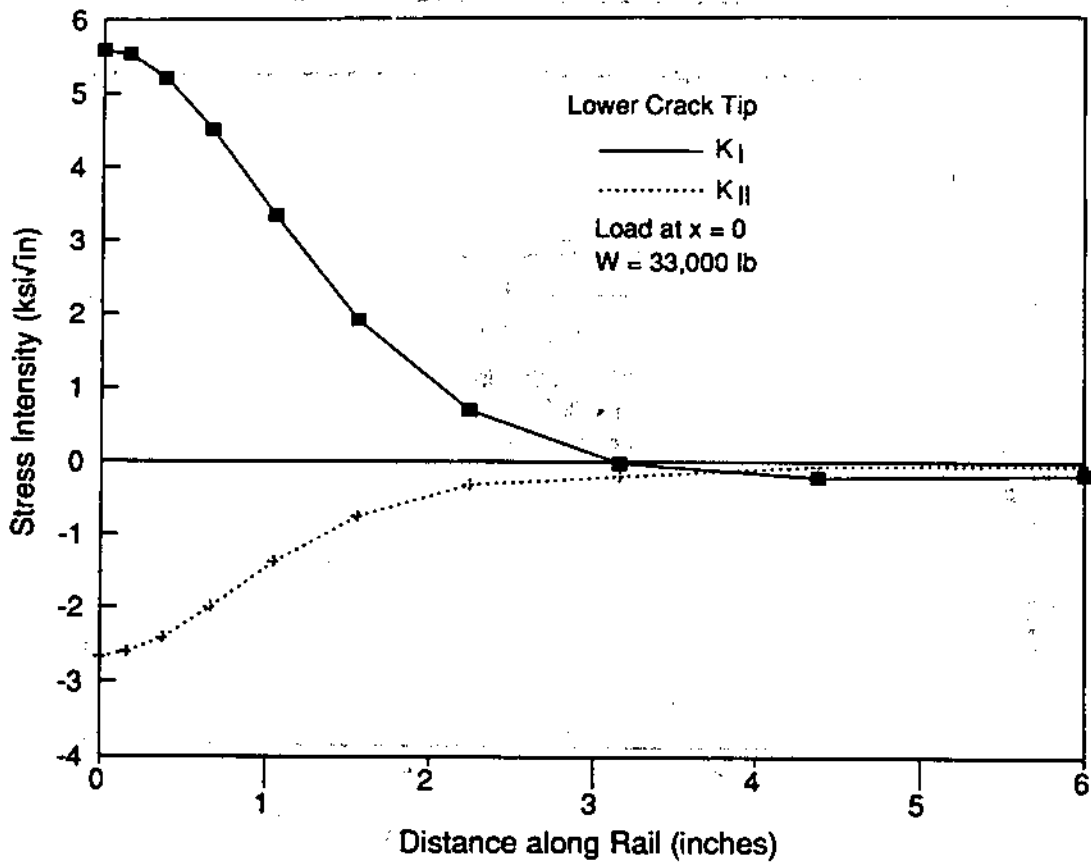
FIGURE 3-9. MODES I AND II STRESS INTENSITY FACTORS FOR THE LOWER CRACK TIP: CENTRALLY LOCATED WHEEL LOAD
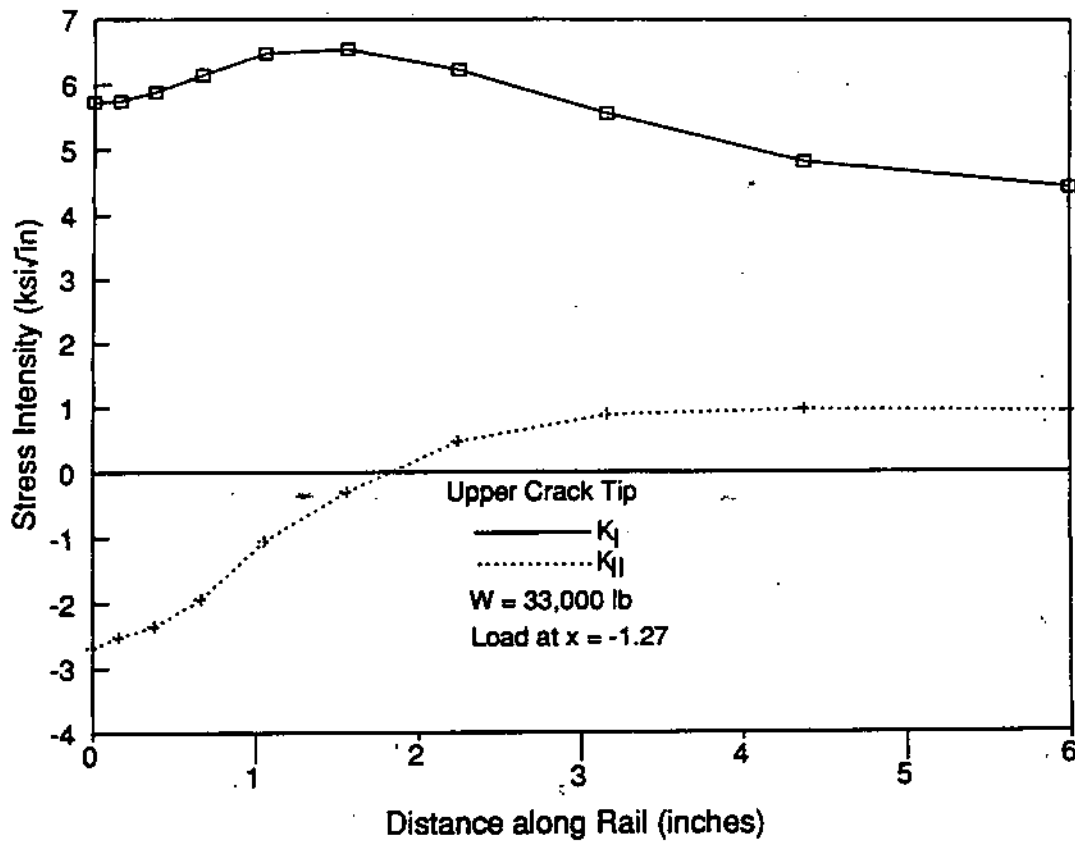
FIGURE 3-10. MODES I AND II STRESS INTENSITY FACTORS FOR THE UPPER CRACK TIP: WHEEL LEAD AT THE RAIL HEAD CORNER
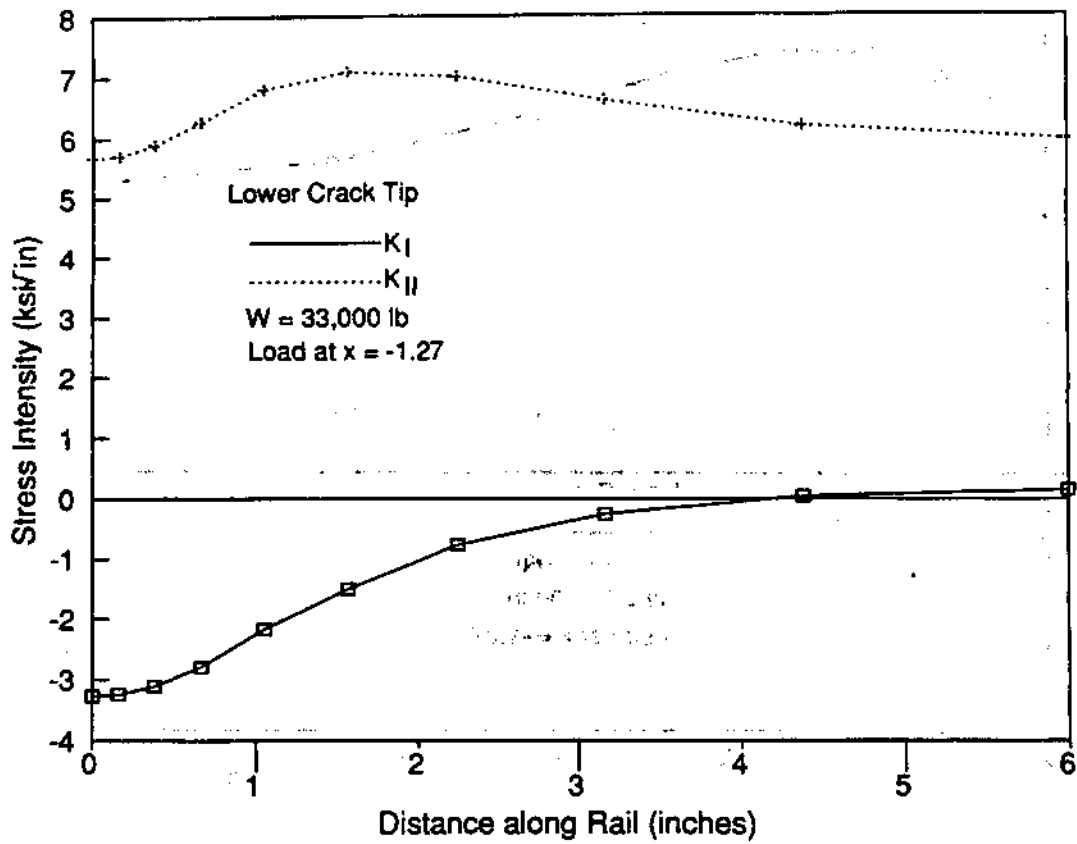
FIGURE 3-11. MODES I AND II STRESS INTENSITY FACTORS FOR THE LOWER CRACK TIP: WHEEL LOAD AT THE RAIL HEAD CORNER

Thus, the maximum Mode I stress intensity factor for the upper angled crack segment and a vertical load applied at the opposite corner is approximately 7 ksi$\sqrt{\text{in}}$. We will show, in the discussion that follows, that this value is consistent with the observed fatigued fracture surfaces of service defects.

Unlike the two-dimensional results, the three-dimensional results show a significant negative, Mode II stress intensity at the tip of the upper crack. A K_{II} with this sign tends to drive the crack toward the running surface. The results for the lower crack tip are more consistent with the two-dimensional results, with a sign of K_{II} that drives the crack toward the head-web fillet opposite the side to which the upper, angled crack segment is oriented.

3.5 FRACTURE CONDITIONS

We now provide an approximate estimate of the defect length that could cause complete fracture of one side of the rail head. Although the exact form of fracture progression is not known, we consider as a lower bound estimate the case in which break-out has occurred to both the running surface and the head-web fillet along the entire length of the defect.

In effect this leads to a structural situation that represents a built-in beam which must support the wheel load, as illustrated in Figure 3-12.

The critical length of breakout can be estimated by assuming that fracture occurs when the limit load for plastic collapse of the beam is attained. Fracture by an elastic process seems unlikely due to the presence of high, longitudinal, compressive residual stresses at the running surface.

The equation for the load required to cause plastic collapse of a beam with rectangular cross section is given by [14]:

$$W = 2bh^2\sigma_f/\ell,$$

where
- W = load applied at the center of the beam,
- b = beam width,
- h = beam height,
- σ_f = plastic flow stress,
- ℓ = free length of the beam.

In our model we take W to be the wheel load. The beam cross-sectional dimensions, b and h, correspond approximately to one-half the rail head width and the rail head height, respectively. To be conservative, we take the flow stress to be equal to the yield strength which for carbon steel rail is 70 ksi. The parameter ℓ corresponds to the length of the breakout, which we assume to apply to both upper and lower free surfaces.
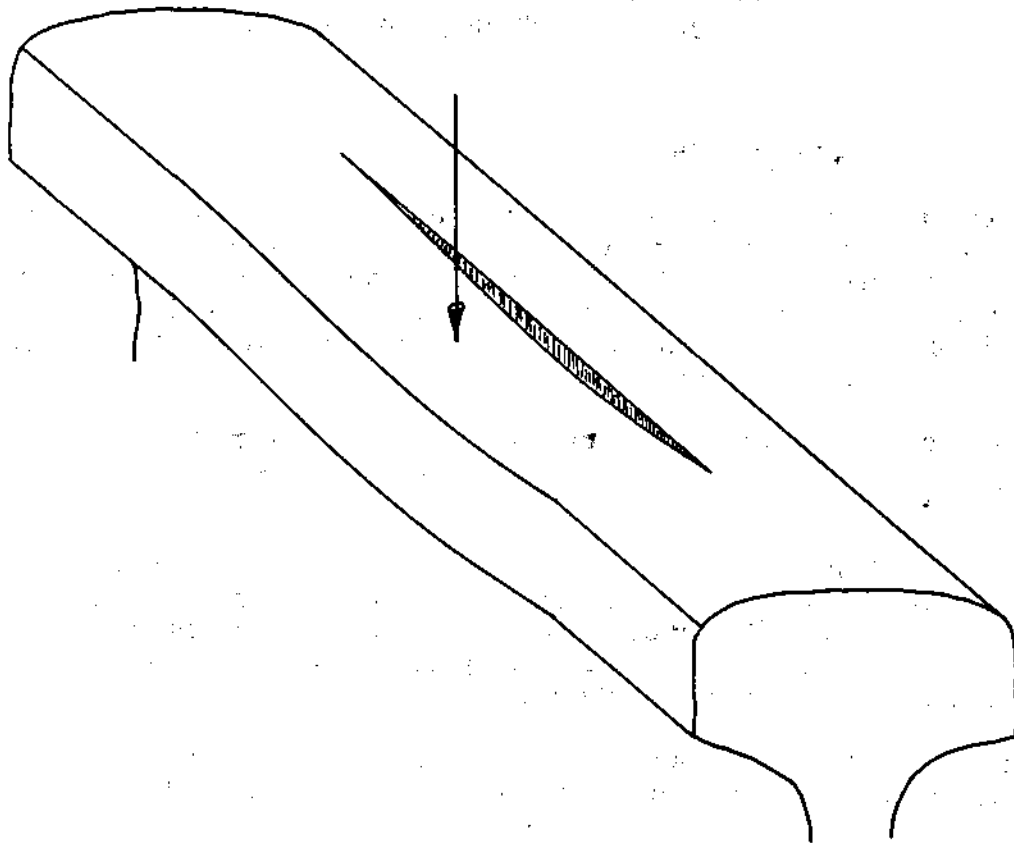
FIGURE 3-12.   **ILLUSTRATION OF THE BEAM MODEL USED FOR ANALYSIS OF COMPLETE FRACTURE CONDITIONS FOR THE VERTICAL SPLIT HEAD**

Thus, an estimate of the critical breakout length can be made. We use a wheel load of 33×10^3 lb and values of b = 1.5 inches and h = 1.5 inches, which correspond approximately to 132 lb/yd rail. Then,

$$\ell = 2(1.5)(1.5)^2(70 \times 10^3)/22 \times 10^3$$
$$= 14.3 \text{ inches.}$$

If the broken out vertical split head intersects a rail end, it acts as a cantilever and the equation for plastic collapse is:

$$W = bh_2 \sigma_f / (2\ell)$$

so that, using the values from the example above,

$$\ell = 3.6 \text{ inches.}$$

The actual value of ℓ for this end case will be greater than this because it is impossible for the wheel load to be concentrated at the very end of the rail; it would also be supported by the other rail end. This argument suggests that the critical defect length is greater than 4 inches.

3.6 DISCUSSION

The results of the three-dimensional finite element analyses indicate that crack growth is very slow from what appears to be the common form of the vertical split head. The alternating stress intensity is only 7 ksi$\sqrt{\text{in}}$ for the defect geometry and loading studied. The R-ratio is also likely to be close to zero, because the very presence of the crack will probably have eliminated the residual stresses transverse to the crack in the plane of the cross section. Add to this the likelihood that the defect is not exposed to the outside environment and the conditions correspond to the threshold fatigue crack growth regime studied by Scutti [15].

Data on fatigue crack growth for rail steel from Scutti show that the crack growth rates for R = 0.05 in vacuum near the threshold are less than 3.9×10^{-8} inches/cycle. We may use this value to estimate the amount of traffic required to cause breakout to the running surface. Thus

Traffic = [0.25 inches/3.9×10^{-8} inches/cycle] x
[2 wheels/cycle] x [33,000 lb/wheel] x [1 ton/2,000 lb]
x [MGT/10^6 tons] = 211 MGT.

This rough calculation demonstrates that the vertical split head, in the form most commonly observed to date, requires a great amount of traffic before breakout to the surface occurs. This explains why vertical split heads are generally discovered before their presence is made known by the observation of a visible crack.

While the finite element analyses provide a basis for the slow growth of the vertical split head, they provide little explanation for the top, angled segment. The two-dimensional results showed essentially no change in K_I for crack angles of 20, 30, and 40°. One might interpret these results as a demonstration that K_I is a maximum at 30° since the crack tip is further and closer to the running surface for the 20 and 40° cases, respectively. However, the distance from crack tip to running surface in these calculations varies from only 0.22 to 0.28 inches; too small a range from which to draw significant conclusions. It may be that the angled portion initiated as a result of the initial, rapid, vertical crack propagation of the defect into a zone of compression, originally present from residual stresses or wheel loading. In any case, the model employed in this study was selected to represent the defect form observed in service.

4. IMPLICATIONS FOR REMEDIAL ACTIONS

The motivation for the investigations just described was to improve the rail defect fracture mechanics models for application to the assessment of remedial actions. We now examine the results of our study to determine their implications for future calculations on remedial actions.

Analysis of the effects of joint bar looseness demonstrate that substantial increases in the bolt hole crack driving force can occur with relatively small degrees of looseness. In fact, driving force becomes large even for joint efficiency factors as high as k=0.6, due to the impact caused by the discontinuity in slope and height at the joint center. Previous analyses [16] were conducted for joint efficiency factors as low as zero. The present study shows that calculations need only be performed for a smaller range, say k= 0.5-0.9, or the maximum k for the joint in question.

The analyses clearly show the benefit of tight joint bars, so that, if not already standard practice, the joint bars should be tightened when a bolt hole crack is discovered. (The slight tendency of tightened head contact bars to encourage crack propogation would be more than compensated by the reduction of dynamic loading.)

Vertical split head defect results from this study show that crack growth is very slow from what appears to be the most common defect shape. This suggests that the usual time required to replace the rail is sufficient and need not depend on defect length or train speed. A different set of criteria would be required for the case in which breakout has occurred and these would certainly include defect length as a parameter. However, preliminary calculations suggest that the length at which different remedial actions should be taken is greater than that specified in the current rules: 4 inches. Further analyses are required to determine these lengths.

5. CONCLUSIONS

A finite element beam model that includes gap elements between rail and joint bars successfully simulates the mechanics of the bolted joint for tight joint bars.

The joint efficiency factor, which is the ratio of the moment carried by the bolted joint to the moment carried by a continuous rail, decreases from 0.85 to 0.6 as the initial gap between rail and joint bars increases from zero to 0.030 inches for 132 lb/yd rail.

A comparable variation in joint efficiency with gap size is obtained for 100 lb/yd rail.

The maximum positive shear force at the first bolt hole under static conditions decreases by ⁻20% as the gap size increases from zero to 0.010 inches for 132 lb/yd rail. This shear force is the driving force for the most commonly observed bolt hole crack which is inclined up and away from the rail end at the first bolt hole.

The modal analysis of the finite element program ABAQUS provides a good method to calculate peak loads in the rail due to impact from a wheel. The use of 10 modes is deemed sufficient when the normalized track damping is $\zeta = 0.10$.

The peak, positive, total shear force at the first bolt hole (including dynamic effects) is predicted to increase by approximately 10% as the rail end height mismatch increases from 0.25 to 0.50 inches for 132 lb/yd rail and a train speed of 10 mph.

The peak, positive, total shear force (including dynamic effects) at the first bolt hole is predicted to increase by approximately 30% as the gap between rail and joint bars and rail increases from zero to 0.010 inches for 100 lb/yd rail and a train speed of 60 mph.

The Mode I stress intensity factor for this loose case is ⁻22.5 ksi√in which is close to lower values of the fracture toughness of rail steel.

The peak, positive, total shear force at the first bolt hole decreases as the rail/joint bar gap size increases beyond 0.010 inches. This is due to the substantial change in contact conditions between rail and joint bars.

Two-dimensional finite element calculations for a vertical split head defect that includes an angled crack segment near the running surface show that the Mode I stress intensity factor is greatest when the wheel load is located at the rail head corner, opposite the side to which the angled segment points.

This maximum K_I for the crack is predicted to be insensitive to the angle of the segment for $\theta = 20$ to $40°$ to the horizontal.

The value of K_{II} for the crack with angled segment is very low where the wheel load is located at the rail head corner, opposite the side to which the angled segment points.

Three-dimensional finite element calculations show that the Mode I stress intensity for the vertical split head with $30°$ angled crack segment is ~7 ksi$\sqrt{\text{in}}$ when the wheel load is at the rail head corner. This value is in the threshold regime for fatigue crack growth and explains the slow growth observed in service.

A 6-inch long model was not sufficient to properly model the vertical split head defect in three dimensions. It appears that at least a 12-inch model is required.

A lower bound estimate of the critical vertical split head crack length is 14 inches for a defect located away from the rail end. The lower bound critical crack length for a defect located at the rail end is 4 inches.

The results show that future calculations to address remedial actions for bolted joints need only consider a narrow range of joint efficiency factors and dynamic amplification for the most common type of bolt hole cracks.

It appears that there is abundant time to remove a discovered vertical split head defect from service without significantly increasing the risk of fracture (assuming that regular inspections have been previously conducted).

It also appears that the range of detected vertical split head defect lengths for which remedial actions are required may be too small.

APPENDIX A

In order to assess ABAQUS's impact modeling capabilities, we first considered the transverse impact of a point mass with a simply supported beam, for which there exists an analytical solution by Goldsmith [7]. The MODAL DYNAMIC procedure, with 20 modes, was used to simulate the impact and ten finite elements were used to discretize the beam. Impact conditions were simulated by imposing an initial transverse velocity to the mass particle. A comparison of model predictions of transverse displacement with the analytical results of Goldsmith is shown in Figure A-1. In this figure, w is transverse displacement, L is the length of the beam, v_0 is the impact velocity of the mass particle, $M=m_1/m_2=1/2$ is the ratio of the total mass of the beam, m_1, to the mass of the particle, m_2, and $a^4=EI/\rho A$, where ρ = mass density and A = cross-sectional area of the beam. The favorable comparison between analytical and numerical results indicated in Figure A-1 suggests that the MODAL DYNAMIC procedure of ABAQUS can provide accurate predictions of beam impact behavior.
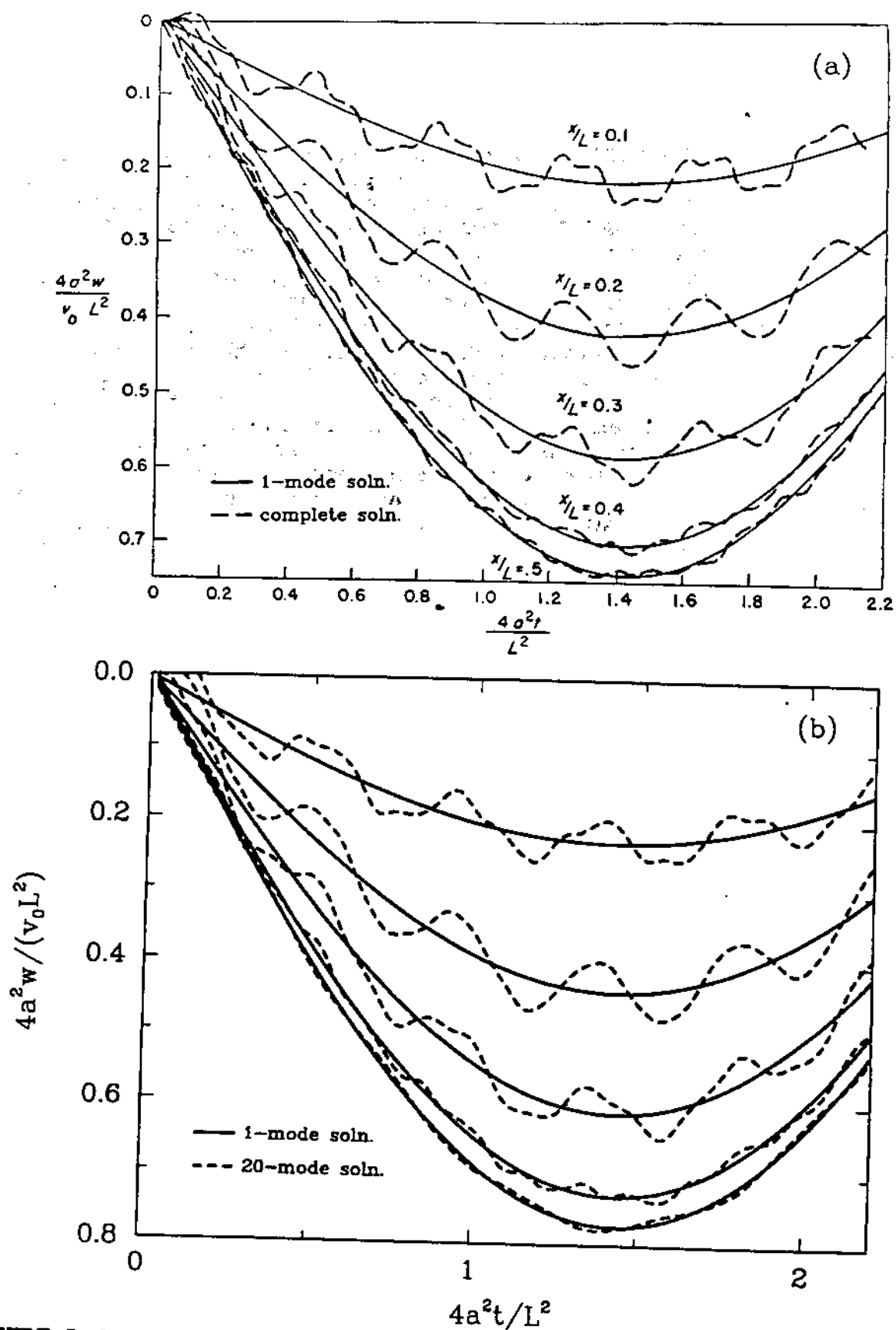
FIGURE A-1. A COMPARISON OF ANALYTICAL PREDICTIONS OF TRANSVERSE DISPLACEMENT (a), TAKEN FROM GOLDSMITH [7], WITH MODEL PREDICTIONS (b).

A-2

REFERENCES

1. Mayville, R.A., P.D. Hilton and D.C. Peirce Investigation of Rail Bolt Hole Cracks. Report to Department of Transportation, Federal Railroad Administration, Contract DTRS-57-83-C-0078, October 1987. .

2. Stresses in Railroad Track - The Talbot Reports. Reprinted reports of the Special Committee on Stresses in Railroad Track, 1918-1940, Prof. A. N. Talbot, Chairman, American Railway Engineering Association 1980.

3. Johns, T.G., S.G. Sampath, J.C. Bell, and K.B. Davies, Engineering Analysis of Stresses in Railroad Rails. Report DOT-TSC-1038, Battelle - Columbus Labs, March 1981.

4. Jenkins, H.H., J.E. Stephenson, G.A. Clayton, G.W. Morland, and D. Lyon, "The Effect of Track and Vehicle Parameters on Wheel/Rail Vertical Dynamic Forces," Railway Engineering Journal, 1974, pp. 2-26.

5. Ahlbeck, D.R., M.R. Johnson, H.D. Harrison, and J.M. Tuten, Measurements of Wheel/Rail Loads on Class 5 Track. Report DOT-TSC-FRA-80-6, February 1989.

6. Timoshenko, S. and B.F. Langer, "Stresses in Railroad Track." J. Appl. Mech., Trans. ASME, 54 (1932), pp. 277-302.

7. Goldsmith, W., Impact - The Theory and Physical Behavior of Colliding Solids, (Edward Arnold; London) 1960.

8. Task Force Report - Rail Failure Evaluation. Report of the Transportation Systems Center for the Federal Railroad Administration, May 1984.

9. Hunt, G.A., "Dynamic Analysis of Railway Vehicle/Track Interaction Forces." Doctoral Thesis, Loughborough University of Technology, June 1986.

10. Mayville, R. A. and P.D. Hilton, Preliminary Investigation into the Fatigue and Fracture Behavior of Longitudinal Defects. Report to DOT-TSC, Arthur D. Little, Inc. Reference 89671, November 1983.

11. Mayville, R.A., Metallurgical and Fracture Surface Analysis of Vertical split Head Defects. Report to DOT-TSC, Arthur D. Little, Inc. Reference 89674, May 1985.

REFERENCES (continued)

12. Mayville, R. A., <u>Crack Growth from Vertical Split Rail Heads</u>. Report DOT-TSC, Arthur D. Little, Inc. Reference 5523, July 1987.

13. Matos, P.P.L, R.M. McMeeking, P.G. Charalambides, and M.D. Drory, "A Method for Calculating Stress Intensities in Bi-Material Fracture". <u>Int'l J. of Fracture</u>, Vol. 40, 1989 pp. 235-254.

14. W. Johnson and P.B. Mellor, <u>Engineering Plasticity</u>, London: Van Nostrand Reinhold, 1973.

15. Scutti, J. J., "Fatigue Properties of Rail Steel." Masters Thesis, Massachusetts Institute of Technology, June 1982.

16. <u>Investigation of the Use of Fracture Mechanics to Set Remedial Actions for Defective Rail</u>. Arthur D. Little Report 61232 to the Volpe National Transportation Systems Center, March 1991.